Universidade de Aveiro Departamento de Biologia
2017

António Luís Ferreira e Pereira

Morfologia e crescimento de estatólitos de bivalves da Ria de Aveiro

Morphology and growth of statoliths from bivalves collected at Ria de Aveiro

DECLARAÇÃO

Declaro que este relatório é integralmente da minha autoria, estando devidamente referenciadas as fontes e obras consultadas, bem como identificadas de modo claro as citações dessas obras. Não contém, por isso, qualquer tipo de plágio quer de textos publicados, qualquer que seja o meio dessa publicação, incluindo meios eletrónicos, quer de trabalhos académicos.

Universidade de Aveiro Departamento de Biologia
2017

António Luís Ferreira e Pereira

Morfologia e crescimento de estatólitos de bivalves da Ria de Aveiro

Morphology and growth of statoliths from bivalves collected at Ria de Aveiro

Dissertação apresentada à Universidade de Aveiro para cumprimento dos requisitos necessários à obtenção do grau de Mestre em Biologia Marinha, realizada sob a orientação científica do Prof. Doutor Carlos Miguel Miguez Barroso, Professor Auxiliar do Departamento de Biologia da Universidade de Aveiro, e da Doutora Susana Galante-Oliveira, Investigadora do Departamento de Biologia e do Centro de Estudos do Ambiente e do Mar da Universidade de Aveiro."

Aos meus Pais.

o júri

presidente

Doutora Ana Isabel Lillebø Batista
Investigadora Principal, Departamento de Biologia & CESAM, Universidade de Aveiro

Doutor Filipe Miguel Grave Laranjeiro
Investigador em pós-doutoramento, colaborador do CESAM, Universidade de Aveiro

Prof. Doutor Carlos Miguel Miguez Barroso
Professor Auxiliar, Departamento de Biologia & CESAM, Universidade de Aveiro

agradecimentos

Gostaria de agradecer a todas as pessoas que de alguma forma me ajudaram na realização deste trabalho.

Ao Professor Carlos Miguez pela excelente orientação e por ter tornado possível a realização deste trabalho.

A Doutora Susana pela imensa ajuda que me providenciou em todas as fazes de elaboração deste trabalho.

A Ana, Joana, Daniela e Belucha e todas as restantes pessoas do LEME, por terem tornado a viagem agradável.

Ao Tiago, pela ajuda no microscópio.

Ao Nito, Rafa e Tito pela ajuda nas saídas de campo.

A todos os meus amigos ainda não mencionados, pela companhia durante estes anos todos.

palavras-chave

Estatocisto, estatólito, moluscos, bivalves, determinação de idade.

resumo

A forma mais comum de estimar a idade de bivalves tem sido a análise de anéis presentes na concha, formados anualmente em resposta a variações sazonais da taxa de crescimento causadas principalmente por alterações de temperatura e disponibilidade de alimento. Há varias limitações a esta metodologia, visto que as conchas estão expostas a elementos de stress físicos e químicos, tornando, por vezes, difícil a determinação da idade. Em espécies comercialmente importantes ou em projetos de conservação, é imperativo possuir meios de determinar com precisão a idade dos animais, sendo o objetivo deste trabalho explorar os estatólitos como estruturas alternativas para a informação da idade.

Considerando as aplicações que têm em outros taxas, os estatólitos de bivalves podem eventualmente ser utilizados para a determinação da idade destes animais, mas este assunto nunca foi abordado na literatura. Por outro lado, é muito escassa a informação sobre morfologia, composição química, cristalografia e crescimento dos estatólitos em bivalves, o que é surpreendente dado que este grupo taxonómico tem sido, desde há muito tempo, intensamente estudado. Assim, este trabalho tenta preencher esta lacuna de conhecimento ao estudar os estatólitos de algumas espécies de bivalves (*Ruditapes decussatus*, *Venerupis corrugata*, *Cerastoderma edule*, *Spisula solida, Solen marginatus, Arcopagia crassa* e *Scrobicularia plana)*, obtidos na Ria de Aveiro ou na zona costeira adjacente (NO Portugal). Um método de extração e processamento de estatolitos de bivalves é aqui apresentado. Dois estatocistos estão presentes perto do gânglio pedal do bivalve, cada um contendo um único estatólito, sendo os estatólitos de cada espécime idênticos na sua forma e tamanho. O aspeto do estatólito destas espécies de bivalves é o de uma pequena esfera translucida e cristalina com anéis conspícuos, não ultrapassando os 70 µm de diâmetro, sendo compostos principalmente por oxalato de cálcio, com vestígios de carbonato de cálcio. Regressões entre o comprimento de concha e o diâmetro de estatólito indicam que os estatolitos acompanham o crescimento da concha, sendo a relação diferente para cada espécie. A utilidade dos estatólitos para a determinação de idade é discutida para as várias espécies estudadas.

keywords

Statocyst, statolith, molluscs, bivalves, age determination.

abstract

The most common way to estimate the age of bivalves has been the analysis of the rings present in the shell, formed annually in response to changes in the growth rate caused by seasonal alterations in temperature and food availability. There are several limitations in this methodology, as shells are exposed to external mechanical and chemical stress, making age estimation difficult or impossible in some cases. In commercially important species or in conservation projects, it is imperative to possess accurate ways to determine the age of the animals, so this work explores the use of statoliths as alternative structures for age assessment.

Considering its current applications in other taxa, statolith characterization might be of great significance in bivalves as they have high ecological and commercial value. Beyond the few studies on its occurrence in Class Bivalvia, the information available in the literature regarding this group is very scarce. Hence, the main objective of this work is to fill the gap in knowledge by studying the statolith in a variety of bivalve species (*Ruditapes decussatus*, *Venerupis corrugata*, *Cerastoderma edule*, *Spisula solida, Solen marginatus, Arcopagia crassa, and Scrobicularia plana)*, collected in Ria de Aveiro or in the adjacent seashore (NW Portugal), and a method for the extraction and processing the bivalve statoliths is here proposed. Two statocysts are present near the bivalve pedal ganglia, each containing a single statolith, their shape and size identical in all specimens. The statolith of these bivalve species appears to be a small, translucent and crystalline sphere with conspicuous rings, diameter no larger than 70 μm, being primarily composed of calcium oxalate, with traces of calcium carbonate. Regressions between shell length and statolith diameter indicate that statoliths accompanies growth in shell, each relation specific for each species. Utility of statoliths for age determination is discussed for each species studied.

Index

Figure index

Chapter 1 – Introduction

1.1 – Introduction

Information regarding the age of organisms is of extreme importance in biological sciences. Reliable ways to estimate age at a certain size, developmental stage or any other moment is important to studies related to species biology and ecology. In this way, it is possible to obtain information such as growth rate, mortality, reproduction and lifespan. It is of particular importance for commercially exploited species since the regulations regarding fishing management is dependent on information based on age. Although there are many ways to estimate age, most rely on the observation of hard body structures such as bones, teeth, shells, etc. In fish, the observation of rings in otoliths, bones and scales have been commonly used for age estimation. In molluscs the shell rings are generally used for age assessment, but recent studies have shown that age estimates can be done reliably by analysis of their statoliths (Arkhipkin, 2005), a structure analogous to fish otoliths. Statoliths are located inside the statocyst and are formed since the larval stage (Barroso et al., 2005; Chatzinikolaou & Richardson, 2007). Each animal possesses two statocysts connected to the nervous system that serve as gravity receptors, an essential part of the general motion of the animal since it provides orientation and equilibrium (Wheeler et al., 2015). Among molluscs, the statolith type and structure can vary greatly. In cephalopods, since most species are highly mobile, their statoliths are larger and more complex than those found in gastropods (Zhang et al., 2015), which are simpler, fitting for their movement characteristics. Although the statoliths in these two groups are extremely different in shape and size, they possess a similar characteristic: they can either be one single statolith present inside the statocyst, or several concretions (statoconia), usually smaller in size. For the past several years, analysis of the cephalopod statolith has provided extremely valuable information regarding growth rates, lifespan and reproductive cycles. Recently, similar studies performed in the gastropod statolith have shown identical possibilities to those found in the cephalopod statolith. In gastropods the occurrence of growth increments in statoliths has been reported in both larvae (Chatzinikolaou & Richardson, 2007) and adults (Barroso et al., 2005), forming growth rings. These increments follow the growth of the animal throughout lifespan and can be used for age estimation and growth studies, while the chemicals present in each ring may prove to be a valuable tool in environmental monitoring as elements and chemical substances present in the water can be trapped in the rings at the time of ring formation (Galante-Oliveira et

al., 2013). Such chemical tagging has been used in fish otoliths (Campana, 1999) as a way to track migration routes, but while fish are highly mobile, a large proportion of the molluscs, in particular the bivalves, are sedentary after larval stage and have a greater potential to act as bioindicators at confined locations.

Even though class Bivalvia includes numerous ecologically relevant and commercially exploited species, tools for management have not evolved beyond the analysis of shells' external surface rings and internal growth lines (Ramón et al., 1995; Peharda et al., 2006; Bagur et al., 2013). These methods' accuracy depends on the correct identification, counting and measurement of periodic growth checks that can be masked by shells' erosion and damage, and even by the deposition of secondary rings, product of the most varied environmental disturbances of either natural or anthropogenic origin (Richardson, 2001). In turn, statoliths are biogenic concretions (in bivalves see Morton, 1985; in gastropods see Galante-Oliveira et al., 2013; in cephalopods see Arkhipkin, 2005) that are, thus, protected from external mechanical and chemical stress. Considering the advantages of their application to study growth, longevity and other individual and population parameters, statolith characterization might be of great significance also in bivalves, group in which information on statolith microstructure and sclerochronological record is lacking.

1.2 – Literature review

The exploration of statoliths in the phylum Mollusca is unevenly distributed. In fact, much work has been done on cephalopods and gastropods, but other molluscs groups are still largely unstudied. A comprehensive revision of the scientific articles (excluding any other type of publication, including review articles) present in the Web of Science database regarding the subjects "molluscan statolith/statocyst/statoconia" revealed 453 results (Fig. 1). These results refer to articles published from 1904 up to September 2017. When analyzing the distribution of the articles per molluscan class, 323 (71.3%) publications were relative to Class Cephalopoda, 112 (24.7%) to Class Gastropoda and only 18 (4%) regarded Class Bivalvia. The remaining molluscan classes were unrepresented. Unsurprisingly, the issues studied in the three named classes differ greatly.

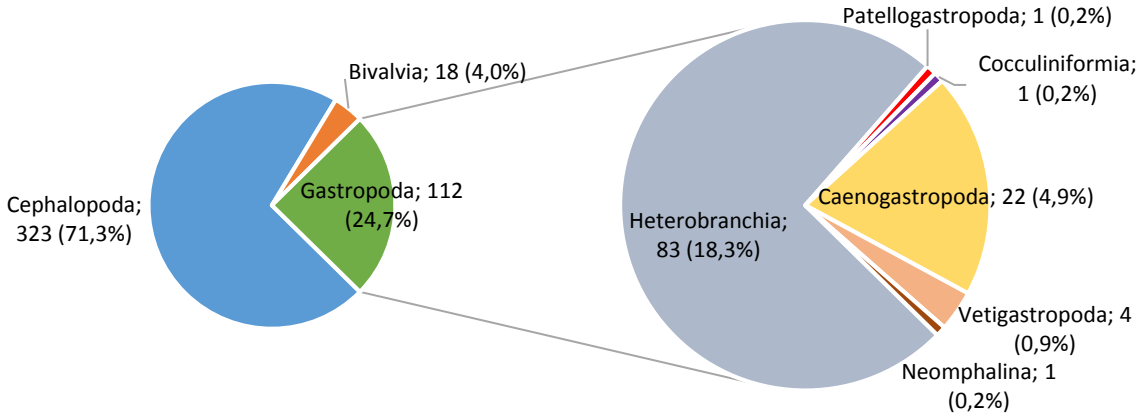

Figure 1 – Distribution of scientific publications, featured on the database Web of Science, on molluscan statocysts/statoliths/statoconia. (Left) Number of publications per class: Cephalopoda (323 publications – 71.3%), Gastropoda (112 publications – 27.7%), Bivalvia (18 – 4%); (Right) – Gastropoda publications per subclass: Heterobranchia (83 – 18.3%), Caenogastropoda (22 – 4.9%), Vetigastropoda (4 – 0.9%), Patellogastropoda (1 – 0.2%), Neomphalina (1 – 0.2%) and Cocculiniformia (1 – 0.2%). Data refers to only standard journal article publications, excluding review articles, short communications, congress papers, conference proceedings, books or book sections.

Cephalopods are the group best described so far regarding the statoliths. Most cephalopods are fast growing and short lived, and they achieve their adult size in a relatively short amount of time, completing their life-cycle from under 8 – 12 months (Forsythe et al., 1994), while longer lived species can go up to 3 years (Forsythe & Hanlon, 1988). Efforts were made to find structures from where information regarding the age of the animal could be obtained. Hard body structures are known to be able to record this type of information. In several species of squids, statoliths were found to have periodic growth marks, and the study of the statoliths' microstructure, followed by chemical analysis of the increments allowed to determine the rate at which these increments are formed for each species (Arkhipkin, 2005). Since the statolith is formed during embryonic stages (Pecl et al., 2010) and continues to grow throughout the animals' lifespan, marks at a quantifiable rate are created (Arkhipkin & Middleton, 2003), making the study of the statoliths' microstructure became extremely important as an aging tool, since it allowed to determine an individual's age essentially at any point in its lifecycle and with extremely high accuracy (Fig. 2). The exception are the species that do not develop a lone statolith mass. For instance, in several species of octopus, instead of a single large calcareous mass, several smaller and 'loosely bound, randomly arranged statoconia are present (Clarke, 1978; Neumeister & Budelmann, 1997)(Fig. 3). Great variety of work has derived from statolith analysis. Since growth marks are formed daily in several squid species, growth rate variations due to climate changes (Arkhipkin et al., 2015; Villanueva, 2000) and acidification (Lacoue-Labarthe et al., 2011; Maneja et al., 2011) can be studied.

Reconstruction of migration routes is possible by analyzing elemental signatures trapped in the growth marks (Liu et al., 2016). Measurement of the distance between rings, as well as the elements sequestered in them, can provide insight in food availability and efficiency (Zumholz et al., 2006; Forsythe, 2004). The major advance in this field has been the refinement of the techniques used to validate statoliths' increments in a greater number of species (Arkhipkin & Shcherbich, 2012). Moreover, several studies have only analyzed a limited spectrum of a species ontogeny and an effort should be made to expand the study of the increments to encompass more life-cycle stages.

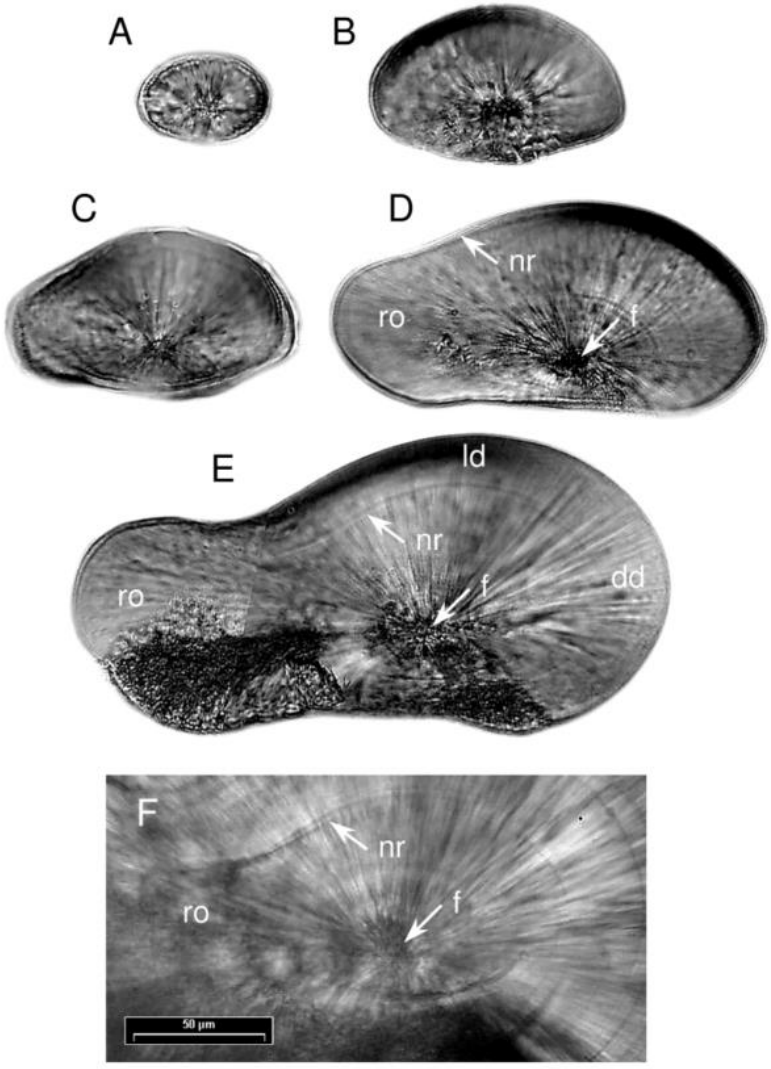

Figure 2 – Morphology of statoliths found in *Loligo gahi* across several stages of their life cycle. (A) Embryo at 23rd stage; (B) Embryo at 27th stage; (C) Embryo at 28th stage; (D) Embryo at 30th stage (hatchling); (E) Paralarva of 4.7 mm mantle length; (F) Juvenile of 18 mm mantle length. Abbreviations for external parts of the statolith: ro, rostrum; ld, lateral dome; dd, dorsal dome; f, internal structure of the statolith; nr, first stress mark (natal ring). Extracted from Arkhipkin & Middleton (2003).

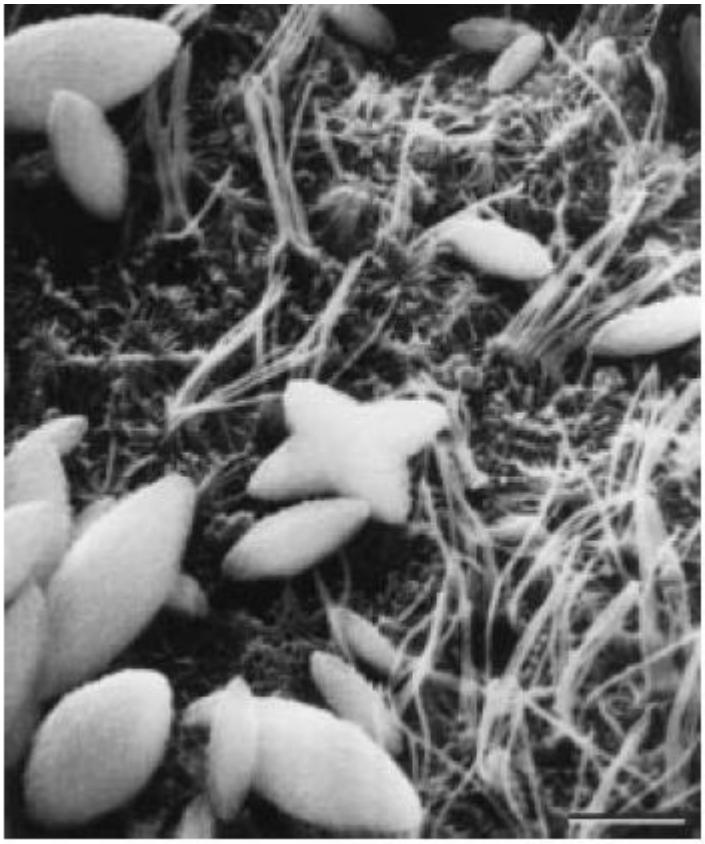

Figure 3 – Scanning electron microscopy image of *Nautilus pompilius* statoconia (scalebar corresponds to 5 μm). Extracted from Neumeister & Budelmann (1997).

Even though studies on gastropod statoliths are not as abundant as in cephalopods, a good number has recently arisen. Gastropods are longer lived than most cephalopods, some species requiring several years to achieve full growth and maturity (Jakubik, 2012). Age determination using shell marks is difficult due to shell erosion, physical damage and repair of the shell (Barroso et al., 2005). As such, discovering other structures where age determination is possible was of great importance in gastropods. Gastropods' statoparticles are much simpler in shape and structure than those present in cephalopods, as is to be expected. Cephalopods are fast moving predators that can perform complex swimming maneuvers. Furthermore, several cephalopod species present large scale and long distance migratory behaviors (Semmens et al., 2007). More advanced and complex orientation or movement assistance organs are, of course, required. In contrast, gastropod species present a much more limited range of motion, therefore a more simplistic gravitational orientation system is sufficient. Two main types of Gastropod statoparticles exist: a single spherical statolith (Grana-Raffucci & Appeldoorn, 1997; Barroso et al.,

2005; Galante-Oliveira et al., 2013; Richardson et al., 2005) (Figs. 4 and 5) or several, usually smaller, statoconia (Pedrozo et al., 1996; Kondrachuk & Wiederhold, 2004; Chia et al., 1981) (Fig.6). Growth marks in the form of concentric rings are present in the statolith as well (Fig. 5). The main challenge to overcome is determining the periodicity of ring formation. Ring formation is dependent on the growth rate of the animal, which varies for each species or even among different populations of the same species (Galante-Oliveira et al., 2013). Still, age determination using statoliths is possible and has been established for several gastropod species. Stronger marked rings are used as they mark significant events in the lifecycles of the animal (Galante-Oliveira et al., 2013). Since statoliths are present from larval stages of the animal (Chia et al., 1981; Grana-Raffucci & Appeldoorn, 1997), the first very strong ring is due to the metamorphosis that occurs while transitioning from planktonic larva to the juvenile stage (Barroso et al., 2005). Afterwards, in temperate regions, since gastropods' growth varies seasonally, annual rings are formed (Chatzinikolaou & Richardson, 2007) and can be used for age estimation. The growth rings also capture the elemental signature of the surrounding environment at time of formation, so are often used for larval dispersion studies (Zacherl, 2005; Manríquez et al., 2012). Gastropods, after metamorphosis, do not move long distances from the general settlement area, and since several species can live up to more than 5 years, their potential as a bioindicator is significant. Other studies on gastropod statoparticles include the determination of initial formation of statoconia, as well as their rate of formation and growth (Kondrachuk & Wiederhold, 2004; Pedrozo et al., 1996), while the general structure of the statocyst can be used in taxonomic classification (Gao & Wiederhold, 1997; Wiederhold et al., 1990).

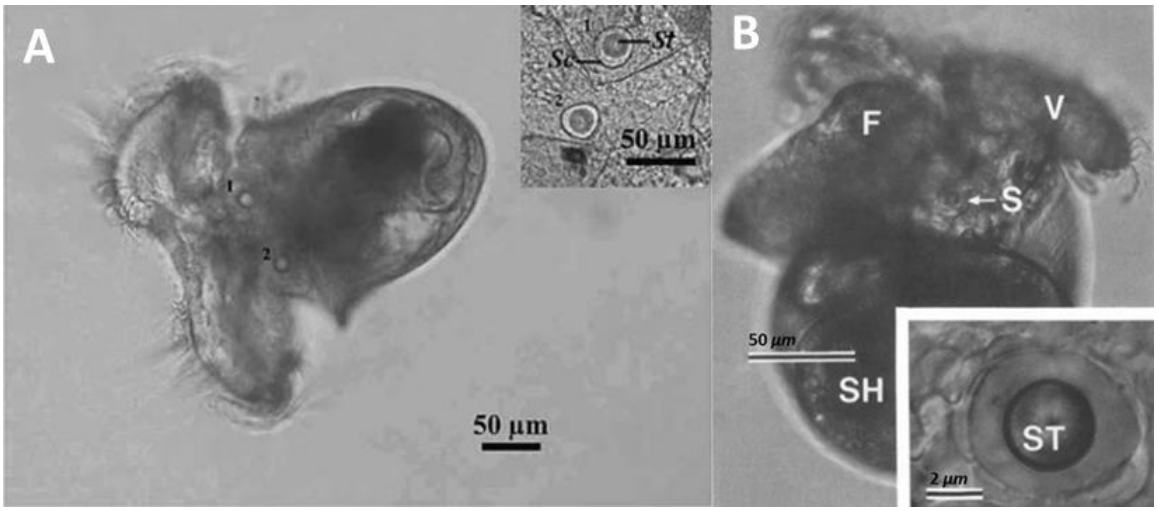

Figure 4 – Statoliths in gastropod veliger larvae: (Left) *Nassarius reticulatus* (Sc – statocyst; St – statolith); (Right) *Rostanga pulchra* (S - statocyst, F – foot, V – velum, Sh – shell; higher magnification of the statocyst shows ST – statolith). Adapted from Barroso et al. (2005) and Chia et al. (1981) respectively.

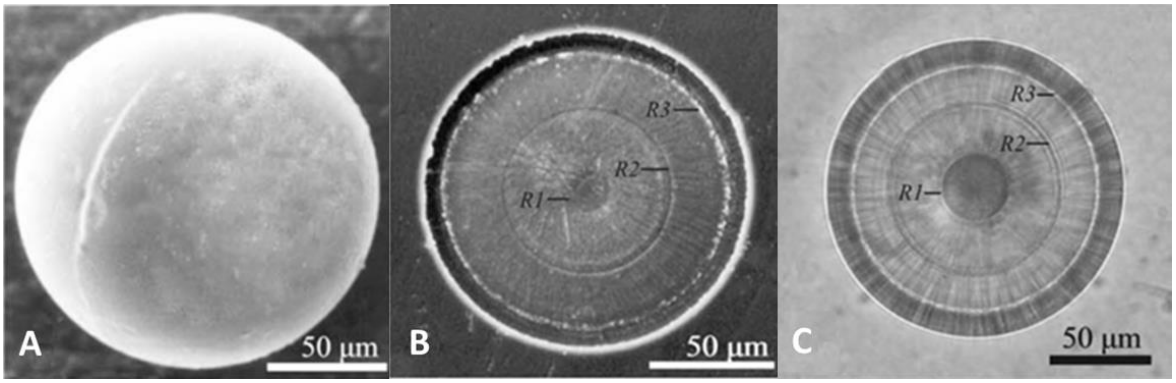

Figure 5 – Scanning electron microscopy images of a statolith of an adult specimen of *Nassarius reticulatus*: (A) whole statolith; (B) sectioned statolith; (C) sectioned statolith under optical microscopy. The first three statolith rings are shown (R1, R2 and R3). Adapted from Barroso et al. (2005).

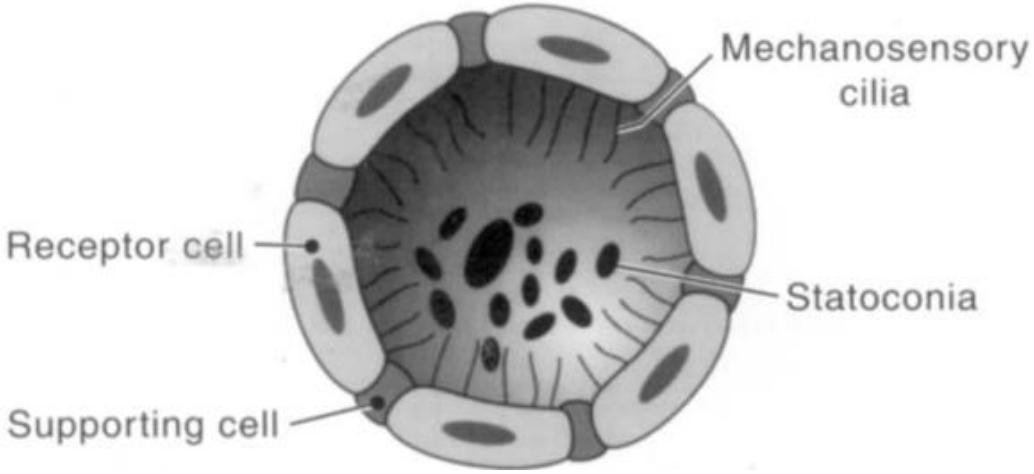

Figure 6 – Illustration of the statocyst of *Aplysia californica*, containing multiple statoconia, several ciliated receptor cells and supporting cells. Extracted from Pedrozo et al. (1996).

Studies regarding bivalve statoliths are much scarcer when compared to the two previous groups. Considering the applications and the advantages that it has brought to the advance of knowledge of other molluscan groups, statolith characterization in bivalves might also be an important step forward. However, knowledge of statoliths in bivalve species is limited to their presence/ absence and type. In particular, Morton (1985) identified three different types of statocysts in the anomalodesmata superorder: types A, B and C.

Type A statocysts were only found in *Pholadomya candida* (Fig. 7). As described by Morton, "the paired statocysts are located in the foot, near the pedal ganglia. Each statocyst is described as an elliptical capsule approximately 150 µm long, 100 µm wide and 10 µm thick. It is surrounded by a

layer of ramified nervous tissue. The nerve endings form small projections on the inner surface of the statocyst and presumably transmit information to a looped nerve that arises as a single root from the anterior most pedal nerve. The statolith is a solid, cellular structure. The inner core comprises a loose syncytium bounded by a thin cuboidal epithelium. The epithelium invaginates at two places to form narrow tubular structures that progressively narrow and bifurcate at their tips. The wide openings to the tubules are at right angles to each other and the tubules themselves are apparently secretory, so that the apertures are blocked by what appear to be secretory droplets. Possibly, the secretions from the tubules of the statolith locally stimulate specific nerve endings for fine position assessment. The tubules of the right statolith project downwards, those of the left are oriented upwards. This opposite orientation possibly confers a sense of dimension in a third plane" (Morton, 1985).

This type of statocyst is much more complex than types B and C. The unique characteristics of this particular type is thought to be an evolutionary adaptation of the species. The complexity of this statocyst points to a need to execute highly coordinated and precise behaviors, unlike those found in most bivalves.

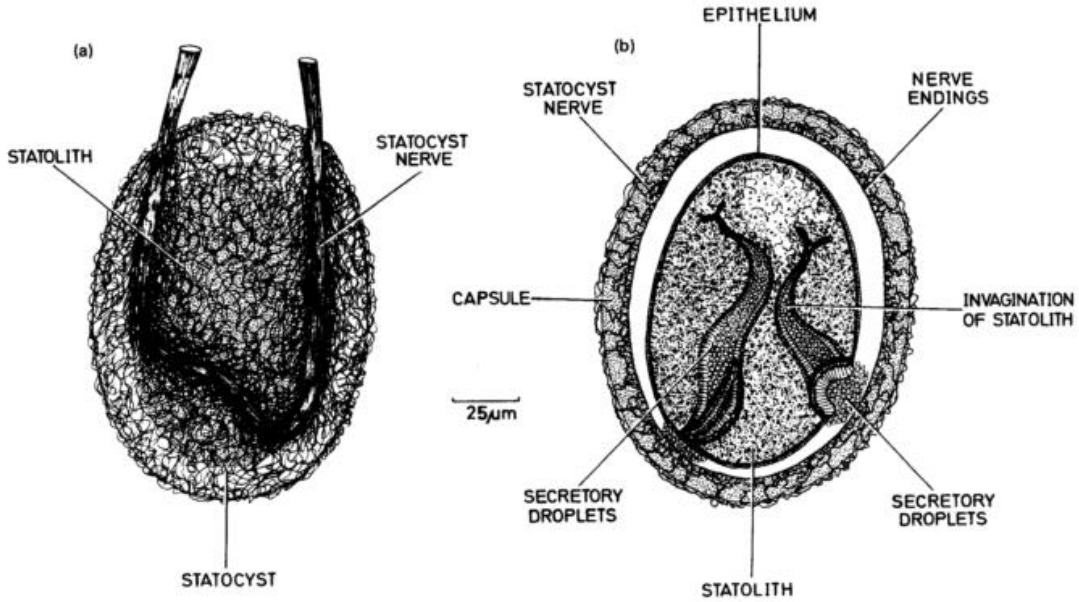

Figure 7 – Type A statocyst found in *Pholadomya candida*: (a) external view; (b) internal view. Extracted from Morton (1985).

The most common type of statocyst, type B, is further divided in 3 subclasses: B1, B2 and B3 (Fig. 8). Type B statocysts are also much simpler than type A, possessing thin cellular layers and an internal epithelium bordered with cilia. The sub-types of statocyst are very similar to each other, with slight variations in the location of the statocyst relative to the pedal ganglia (i.e, adjacent or separated to the pedal ganglia), but mainly differing in the type of statoparticles present inside the statocysts itself: type B1 has a single statolith inside each statocyst; type B2 presents several smaller statoconia and a single, larger statolith; type B3 presents more irregularly shaped statoconia, with again one statoparticle being slightly larger, but does not have the same shape as those present in types B1 and B2.

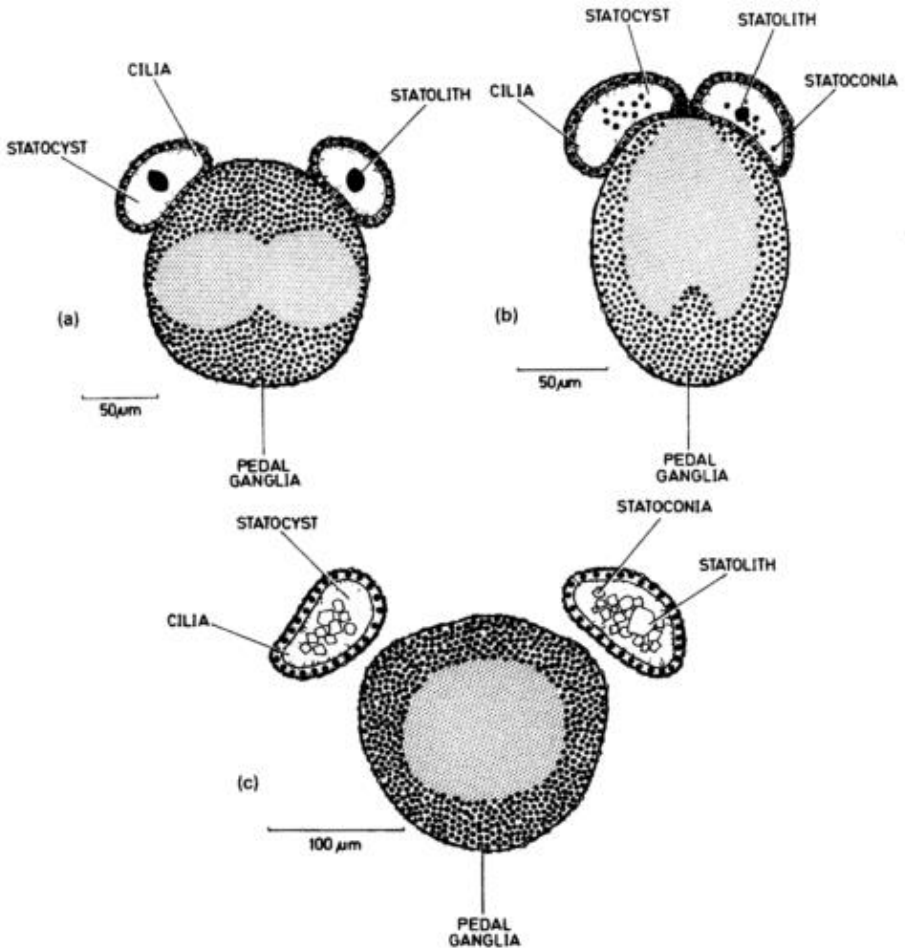

Figure 8 – Transverse sections of type B statocysts: (a) Type B1 (*Thracia villosiuscula*); (b) type B2 (*Myadora boltoni*); (c) type B3 (*Myadora striata*). Extracted from (Morton, 1985).

Type C statoliths (Fig. 9) are positioned at a larger distance of the pedal ganglia than the previous types. They are composed of comparatively larger cells (4-5). The nucleus are located in a corner of the cell, giving the impression of a large empty space being present. The cilia observed in previous types are replaced by small microvilli. A single statolith is present in each statocyst, comparatively larger than in previous types, occupying much of the internal space available.

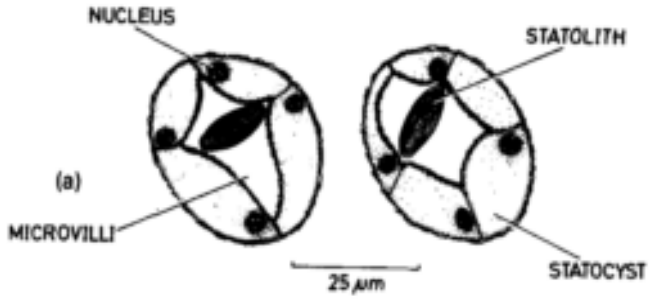

Figure 9 – Transverse section of type C statocysts: (a) Type B3 statocyst (*Cuspidaria suganumai*). Adapted from (Morton, 1985).

Bivalve statoliths were described in several other species as well, on occasion being also used as a means of taxonomical classification (Cragg & Nott, 1977; Young et al., 2003). Occasional references to bivalve "statoliths" are found in few species' morphoanatomical description, among them *Minnivola pyxidatus* (Morton, 1996) and several other species in the *Anomalodesmata* superorder (Morton, 1985). Barber and Dilly (1969) details several aspects of the statocysts in the genus *Pecten* and *Pterotrachea*, and analyses multiple aspects of the cellular structure that the statocysts are a part of. Passos and Machado (2014) describe a new species in the *Cyamiidae* family (*Cyamiocardium domaneschii*), detailing as well the type of statocyst present. Sartori and Domaneschi (2005) studied the functional morphology of *Thracia meridionalis* and report two statocysts near the pedal ganglia.

While these studies may describe in detail the location, type and function of the statocysts and their statoparticles, they do not examine their microstructure, chemical composition, growth or the possibilities for age estimation.

1.3 – Objectives

The work's primary goal is to contribute to the knowledge of the statoliths of the class Bivalvia. The focus is to provide new insights regarding statolith location, morphology, micro-structure,

elemental composition, growth and potential as an age estimation tool. The species chosen for this endeavor were *Ruditapes decussatus*, *Venerupis corrugata*, *Cerastoderma edule*, *Scrobicularia plana*, *Solen marginatus*, *Spisula solida*, *Arcopagia crassa*, *Mytilus galloprovincialis* and *Crassostrea gigas*, all collected from natural populations or aquaculture facilities in Ria de Aveiro and adjacent seashore (NW Portugal).

Chapter 2 – Material and Methods

2.1 – Sampling

2.1.1 – Specimens acquisition

Bivalve specimens were acquired several moments during the years of 2015-2017 in the region of Aveiro (NW Portugal). The anatomical location of statocysts and external appearance of statoliths were studied in *R. decussatus*, *V. corrugata*, *C. edule*, *S. plana*, *S. marginatus*, *S. solida*, *A. crassa*, *M. galloprovincialis* and *Crassostrea gigas* (adult and larvae). Additionally, statolith diameter (StD) *vs* shell length (SL) regressions were investigated in four of the above mentioned species (*R. decussatus*, *V. corrugata*, *C. edule* and *S. plana*) and electron microscopy and Micro-Raman spectra were performed in the clam *R. decussatus*. All specimens acquired were kept frozen at -20°C until further processing.

2.1.2 – Specimens from natural populations

S. plana was captured in February and March 2017 (n = 74, from 4 to 50 mm SL, 26.55 ± 16.46 mm SL) in Canal de Mira. *Cerastoderma edule* (n = 54, average SL = 13.56 ± 8.21 mm), *M. galloprovincialis* (n = 20, from 5 to 30 mm SL), *A. crassa* and *S. marginatus* were captured in September 2016 in Canal de Mira as well. These species were collected in the intertidal area by hand or using a shovel during the low tide. *S. solida* was obtained from a local bivalve purification center, with the guarantee that they were cached from the Aveiro seashore. *Crassostrea gigas* adult specimens of various sizes (n = 20, 5 - 30 mm SL) were obtained from a local aquaculture production (extensive regime) in Costa Nova, Ria de Aveiro (NW Portugal). *R. decussatus*, *V. corrugata* and *C. gigas larvae* were obtained from a nursery in Ria de Aveiro.

2.1.3 – Specimens from aquaculture facilities

As mentioned before, *R. decussatus* and *V. corrugata* specimens used in this study were obtained from a local shellfish nursery in Ria de Aveiro. The nurseries' project strived to grow clam seed of both species following a semi-intensive regime in a floating upwelling system (FLUPSY, see Chessa et al., 2013). Clams were kept in silos attached to a floating structure as shown in Fig. 10. An upwelling current created by a motorized mill passes upwards through screened openings in the bottom of the silos. This type of system has several production advantages for clam seed growth, such as allowing for high stocking densities while keeping both water flow and food intake at

sufficient rates. In addition, since the clams are kept in silos, predation almost nullified as there are no easily accessible entry points. This type of system, however, requires that several key conditions be maintained. A large and controlled water body is necessary for the floating structure, with the capability to assure water renovation as well. Supply of additional micro algae is recommended to keep nutrient flow constant and ingroove growth rate of the clams, as natural micro algae supplies might be lacking and are more dependent on climate variations. However, heavy algae blooms or any large amount of suspended water particles are undesirable, since they can clog the silos' mesh, restricting the upwelling flow. Due to the particular requirements of this type of system, frequent maintenance of the silos and control of the production is needed. Evolution of hydrological parameters was registered – temperature and oxygen concentration in water (Cº and mg/L respectively; measured with an oximeter, Oxyguard Handy Polaris), salinity (‰; measured with a portable hand refractometer, Zuzi model C-1).

Two batches of *R. decussatus* seed (initial SL≈ 2.5 -3.5 mm) arrived at the nursery on the 3rd of November 2015, obtained from a hatchery in the Netherland. Each batch was composed of distinct spawns: the first originating from Dutch breeders (Dec_H), while the second was obtained from Portuguese breeders (Dec_PT, captured earlier in the same year from Ria de Aveiro) specifically sent to the hatchery for spawning. Dec_H and Dec_PT were maintained in separate silos, but under the same growth conditions. Specimens selected for statolith observation were of a wide range of sizes and their collection was done in three moments: December 2015 (Dec_H SL ≈ 2.64 - 5.86 mm, n = 60; Dec_PT SL ≈ 4.00 - 13.57 mm, n = 90), March 2016 (Dec_H SL ≈ 2.57 - 16.73 mm, n = 60; Dec_PT SL ≈ 3.00 - 15.34 mm, n = 60) and July 2016 (Dec_PT SL ≈ 9.34 - 27.64 mm, n = 23). Due to heavy mortality during the Spring months, no Dec_H specimens were collected in July. Hence, total number of specimens sampled for statolith observation were: 120 from Dec_H, 173 from Dec_PT.

The *V. corrugata* batch arrived at the nursery in April of 2016 from the same hatchery, spawned from Portuguese broodstock. Sampling of specimens for statolith observation was conducted in April 2016 (n = 38, average SL = 7.43 ± 4.753 mm) and again in September 2016 (n = 20, average SL = 12.87 ± 1.422 mm).

C. gigas larvae were supplied from same hatchery in the Netherlands. Larvae were approximately 17 days old (pediveliger stage), preserved in absolute ethanol.

Figure 10 – Nursery in the Ria de Aveiro. (A) Floating upwelling systems – FLUPSY's. (B) FLUPSY silos fixed in pairs; (C) Low stocking conditions of *R. decussatus* clam seed; (D) High stocking conditions.

2.2 – Statolith extraction

Statoliths were extracted from the pedal ganglia region (Fig. 11 and 12) of the bivalves under study.

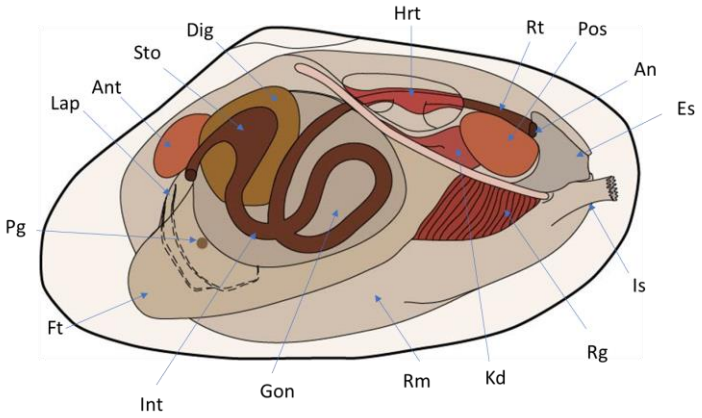

Figure 11 – General clam anatomy, under the description by Gosling (2003). An – anus; Ant – anterior adductor muscle; Es – excurrent siphon; Dig – digestive gland; Ft – foot; Gon – gonad; Hrt – heart; Int – intestine; Is – incurrent siphon; Kd – kidney; Lap – labial palps; Pg – pedal ganglia; Pos – posterior adductor mucle; Rg – right gill; Rm – right mantle; Rt – rectum; Sto – stomach.

After thawing, SL was measured and the soft tissues removed by cutting the adductor muscles. In specimens of extremely small sizes (SL between 3 and 7 mm, approximately), due to low tissue density, lightly squeezing the soft tissues between glass slide and cover slip can reveal the pedal ganglia and statocysts under light optical microscope (OM) at 100x magnification, the statoliths' diameter StD measurable at 400x. In larger specimens, however, the soft tissues were submitted to a controlled digestion (duration dependent on the animals' size and species, from 30 minutes to 2 hours) by immersion in a 1:1 mixture of 35% H_2O_2 and 0.1N NaOH in distilled water to facilitate the location of the pedal ganglia. On several specimens, particularly in *S. solida*, the pedal ganglia is promptly detectable even in large specimens, without prior soft tissue digestion, by simple observation under a stereo microscope (Fig. 12 C). Removing unnecessary soft tissues and carefully harvesting the general area around the pedal ganglia facilitates tissue digestion, especially useful in larger specimens were digestion's duration is more time consuming. After achieving the desired tissue transparency and malleability, sufficient for the identification of the pedal ganglia within the foot, the remaining tissue was rinsed in distilled water. On juvenile specimens (SL between 7 and 17 mm, approximately) the remaining tissue was slightly squeezed between glass slide and cover slip to determine statocysts' location. However, in specimens of greater size, particularly in *R. decussatus* species, tissue density was usually too much to allow statocysts' detection. At this point, caution should be exerted in extending digestion duration for too long, as statolith surface can be damaged by the process. In specimens where statocysts were not readily visible, tissue surrounding the pedal ganglia was carefully "excavated" using fine tweezers and regular beveled needles until statocysts' detection. In all cases, two statocysts were

identified per animal, each containing a single spherical statolith. The smallest piece of tissue (possible to manipulate) containing both statocysts was harvested and placed in a watch glass. Smaller statoliths (StD inferior to 25 µm) were digested in pancreatin following Álvarez-Padilla and Hormiga (2007), (Fig. 13). In statoliths of greater size, each statocyst was ruptured using hypodermic beveled needles and each statolith gently led out of the statocyst. Finally, released statoliths were rinsed in distilled water by pipetting, and preserved in absolute ethanol until further processing. For micro-structure analysis, structures were left to dry at room temperature in closed Petri dish inside a desiccator, and then mounted in glass slide. For more accurate StD measurements, some structures were mounted in glass slide with cover slip in DPX mounting medium, observed under OM at x1000 magnification (oil immersion lens), focused in their middle plane a, photographed using a MOTICAM model 2300 and measured with the respective software.

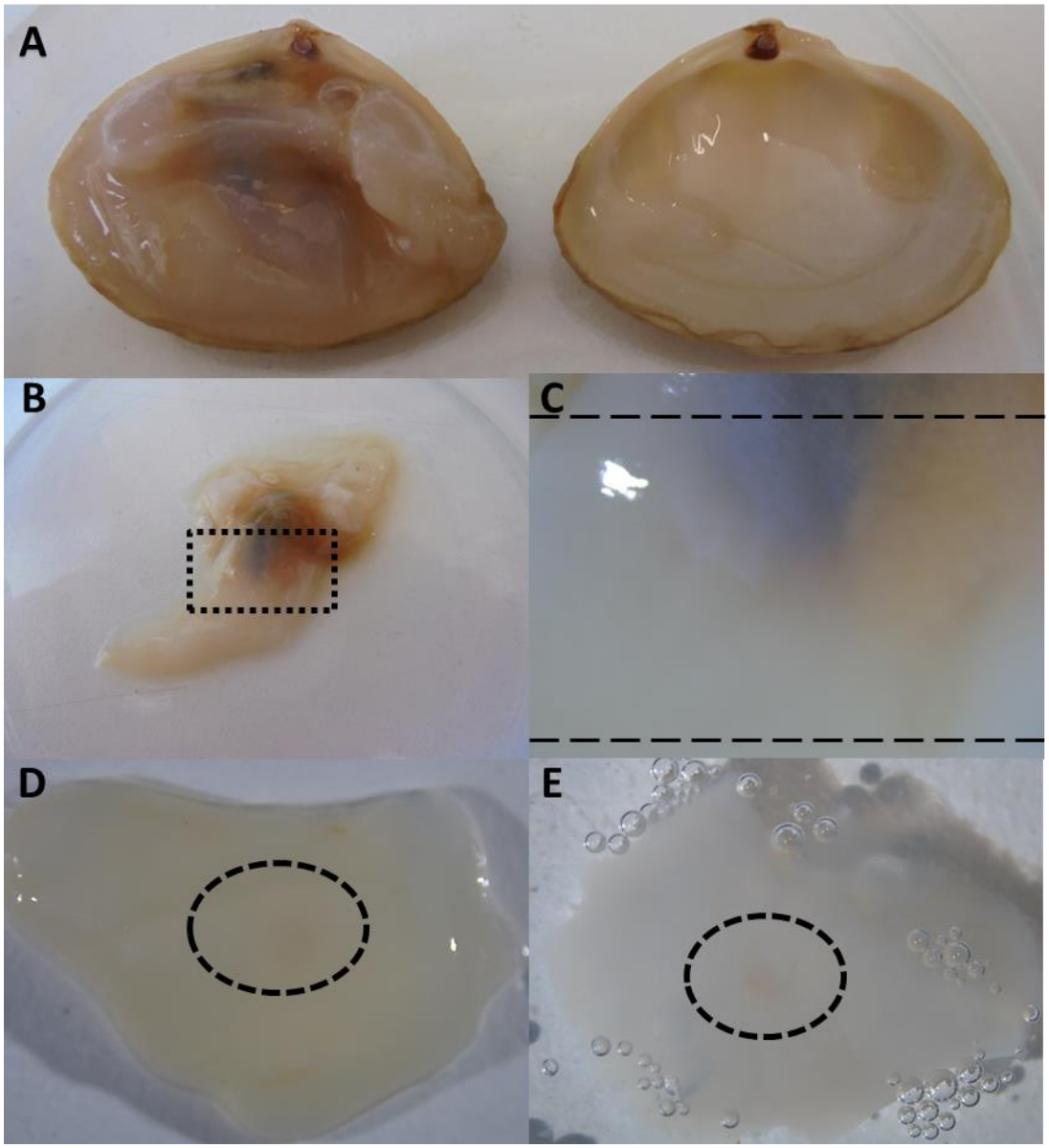

Figure 12 – Statolith extraction in *S. solida*: (A) Clam shell separated by cutting of the adductor muscles; (B) General region of the body where the pedal ganglia is located; (C) Dotted line details recommended cut to separate rest of body from foot; (D) Piece of tissue containing visible pedal ganglia under stereomicroscope; (E) Same piece of tissue after 30-60 min. digestion by immersion in a 1:1 mixture of 35% H_2O_2 and 0.1N NaOH in distilled water.

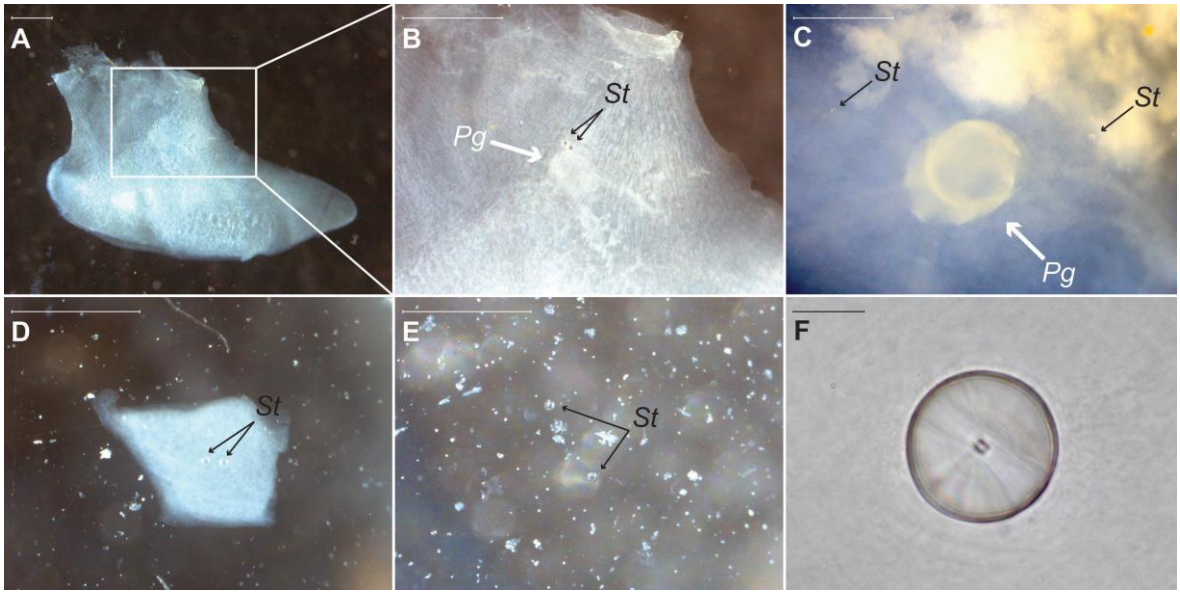

Figure 13 – Extraction and processing of statoliths from *R. decussatus* foot: (A) Foot after ≈2 hours' digestion in 35% H2O2 and 0.1N NaOH (1:1); (B) Location of pedal ganglia (Pg) and statocysts containing statoliths (St); (C) Detail of Pg and St; (D) Section of tissue containing St under pancreatin digestion; (E) St released from soft tissues after ≈1.5 hours' digestion in pancreatin; (F) St focused in its middle plane at 1000x magnification. Scale bars in A-E correspond to 0.50 mm, and in F to 10 µm.

2.3 – Statolith diameter (StD) and shell length (SL) relationships

Following the protocol described previously, SL was measured using a calliper and StD was measured with a light optical microscope at 400x magnification. The StD of the paired statoliths were plotted against each other, to determine if there are differences in size between the two. Afterwards, and knowing that there was no significant difference between left and right statoliths, one statolith per animal was chosen (at random) and the StD was plotted against the respective SL.

2.4 – Electron Microprobe Analysis

Statoliths were extracted from 10 *R. decussatus* specimens obtained from July 2016, a single statolith per clam was used. A drop of HCl (0.1 M) was dropped on two statoliths for approximately 30 to 40 seconds, washed afterwards with distilled water by pipetting. Specimens were then mounted in carbon tape and Carbon-coated to guarantee the material electrical conductivity for the acquisition of secondary electrons images (SEI) in a JEOL 8500-F electron probe microanalyzer equipped with a high sensitivity SDD-type Energy Dispersive Spectrometer. Some of these structures were broken with a scalpel in order to obtain fracture planes of untouched matrix (i.e., surfaces that had not been in contact with any treatment used during extraction and cleaning procedures). The general composition was then assessed by the carbon

coated surfaces' through the acquisition of energy dispersive X-ray spectra (EDS) for 30s at an acceleration voltage of 10 kV and a beam current of 10 nA, in a significant area of each sample.

2.5 – Micro-Raman Spectroscopy

Raman spectra were acquired in two statoliths extracted from two different *R. decussatus* individuals, following the methods previously described by Galante-Oliveira et al., (2014). Structures were manually removed from the statocyst using hypodermic needles, rinsed in absolute ethanol by pipetting, placed in a concave slide inside a covered petri dish (to limit air suspended particles' deposition to a minimum) and left to dry at room temperature inside a desiccator. After cleaning and prior to spectra acquisition, one of the two statoliths was smashed, and the other fractured near its central plane, using a scalpel. Samples were observed using an Olympus microscope equipped with 10, 50 and 100x objectives, part of a Horiba Jobin Yvon LabRam 800HR Raman system. Spectra were acquired by the means of a 532 nm line of a Quantum Ventus laser up to 20 mW, a 100x (N.A. 0.9) objective, a grating with 1800 grooves mm^{-1} and a pinhole of 200 µm. Spectra were acquired randomly in the smashed statolith and in fracture planes in the fractured statolith (approximate location in Fig. 14), at a resolution of approximately 2 cm^{-1} in the range between 70 and 3800 cm^{-1}. Repeated acquisitions of each spectrum were accumulated (10 scans of 30s each) to improve resolution.

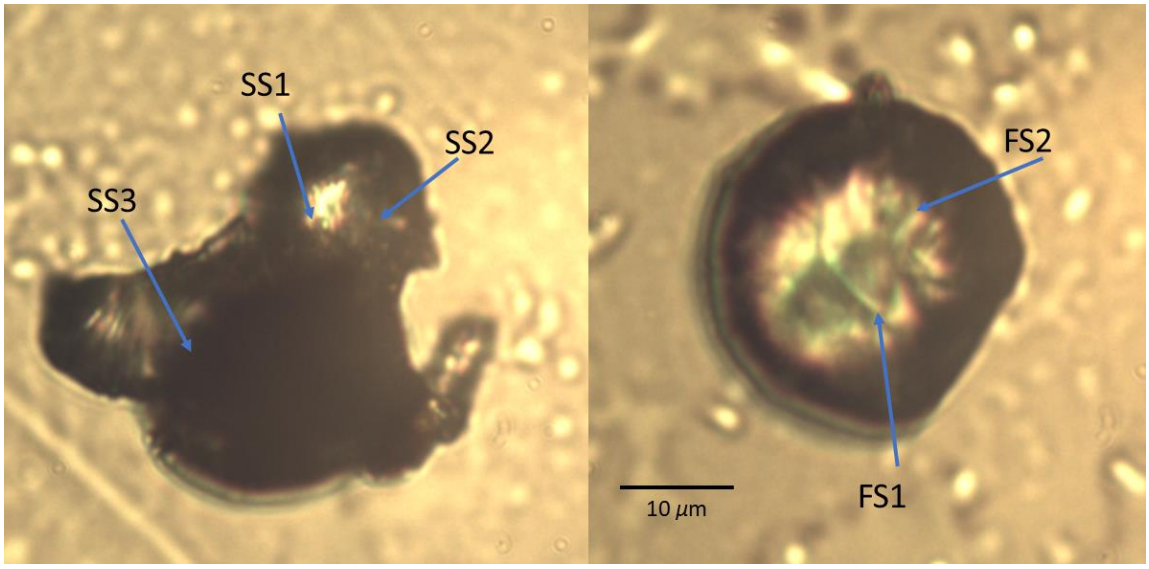

Figure 14 – *R. decussatus* statoliths. Optical microscopy (OM) photographs of the structures in which Raman spectra were acquired, at 400x magnification. Blue arrows indicate the locations at which spectra were acquired. (Left) 3 spectra in the smashed statolith (SS1 to 3); (Right) 2 spectra in the fractured statolith (FS1 and 2).

Chapter 3 – Results and Discussion

3.1 – Statocyst structure and location

Statocysts were localized, in all cases, near the pedal ganglia of the specimen. The location of the pedal ganglia differs very slightly between the species. For instance, in *V. corrugata* the pedal ganglion was usually found anteriorly to the gonad and intestines (Fig. 15) while in *R. decussatus* and *S. solida* it is usually found in a more ventral position to the same organs (see Fig. 12 in Material and Methods section).

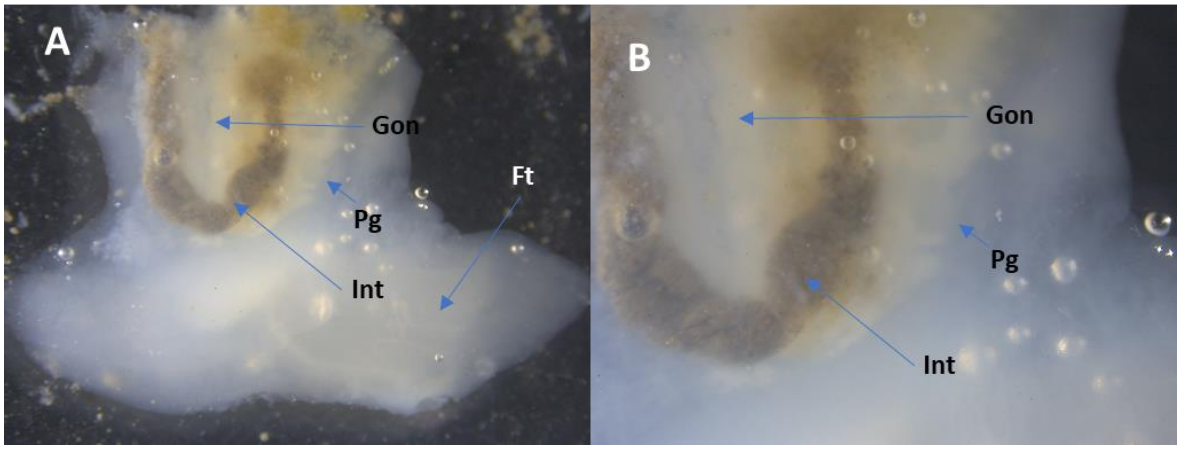

Figure 15 – *V. corrugata* digested tissue, observed under stereomicroscope. (A) – Overview of the tissue, containing the foot (Ft), part of the gonad (Gon), intestines (Int) and location of pedal ganglia (Pg); (B) – Closer view of the region containing the pedal ganglia (Pg).

In *S. marginatus*, who possesses a more distinct body structure when compared to the other clams studied, the pedal ganglion is located on the posterior end of the foot, laterally to the intestine and style sac (Figs. 16 and 17).

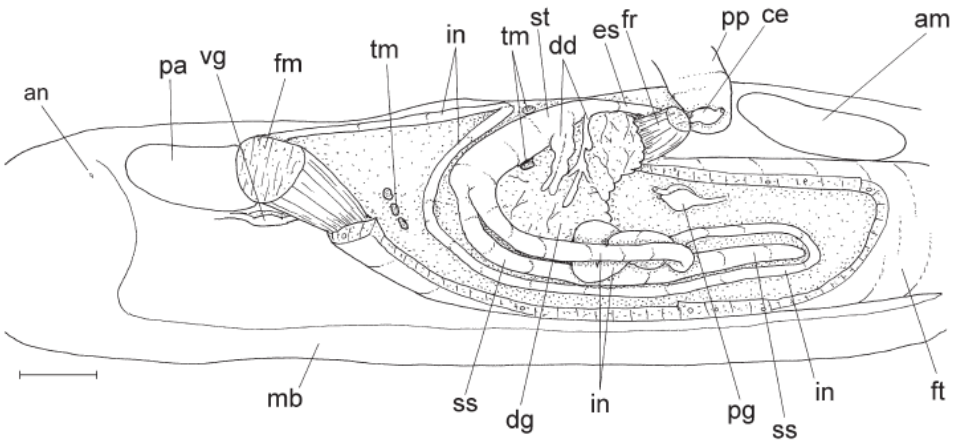

Figure 16 – Anatomy of *Solen exiguus* showing whole right view with shell removed, to show location of the pedal ganglion in the *Solen* genus. Abreviation: am - anterior adductor muscle; an: anus; ce: cerebral ganglion; dd: ducts to digestive diverticula; dg: digestive diverticula/gland; es: esophagus; fm: posterior foot retractor muscle; fr: anterior foot retractor muscle; ft: foot; in: intestine; mb: mantle border; pa: posterior adductor muscle; pp: palp; pg: pedal ganglia; ss: style sac; st: stomach; tm: transversal muscles of visceral mass; vg: visceral ganglia. Adapted from Simone (2009).

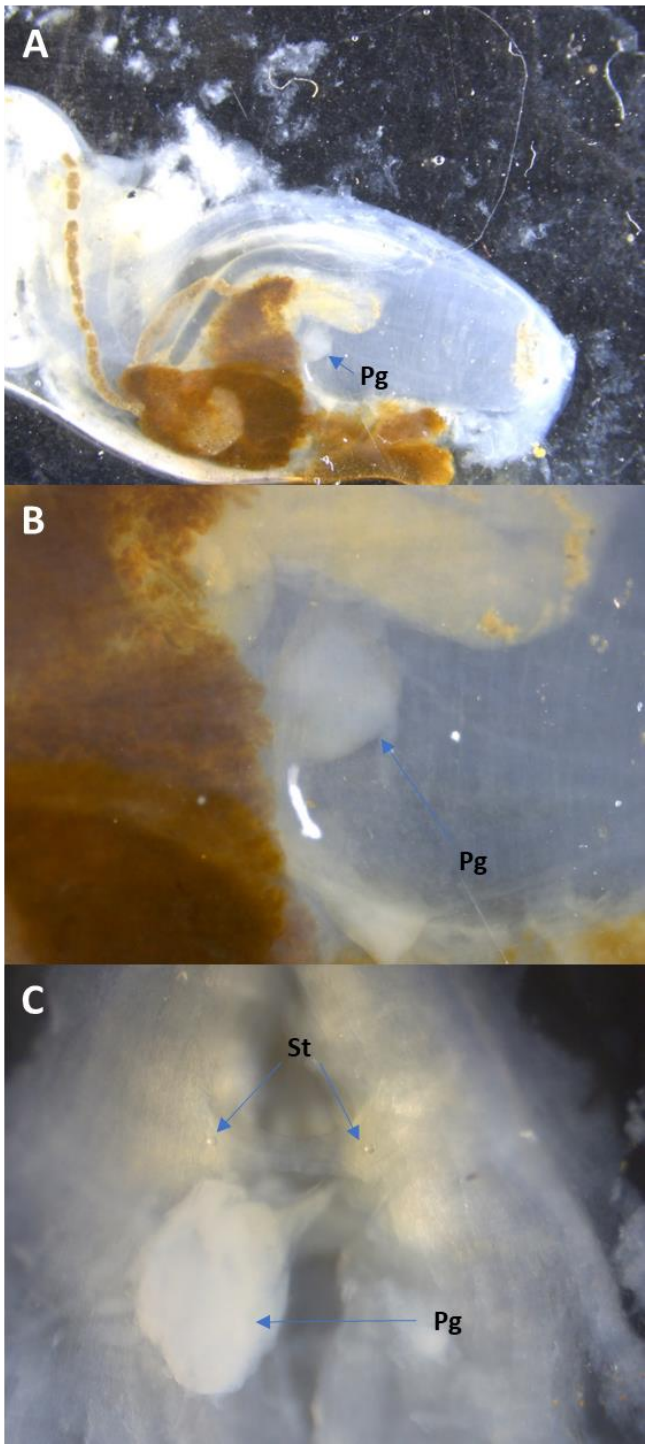

Figure 17 – *S. marginatus*, squeezed between glass slide and cover slip, observed under stereomicroscope: (A) and (B) show the location of the pedal ganglion (Pg); (C) Transversal cut of the piece of tissue containing the pedal ganglion and pair of statoliths.

The color of the pedal ganglia varies among species as well. In *R. decussatus* and *V. corrugata* the pedal ganglia is whiteish, lacks distinction in color from the surrounding soft tissue. In *A. crassa* and *S. solida* for instance, the ganglia are colored (salmon and orange respectively, see Figs. 18

and 19) and easier to find. Localization of the pedal ganglia is much simpler in smaller specimens than in larger ones. Although the ganglion itself is small in size, the lower density of the remaining soft tissues has a much greater influence on facilitating the localization of the ganglion. Consequently, due to the greater density and lack of malleability of the soft tissues in older specimens the ganglion is much harder to find. The color of the ganglion is, therefore, of particular importance in larger specimens, since a more distinctly colored ganglion is much easier locate.

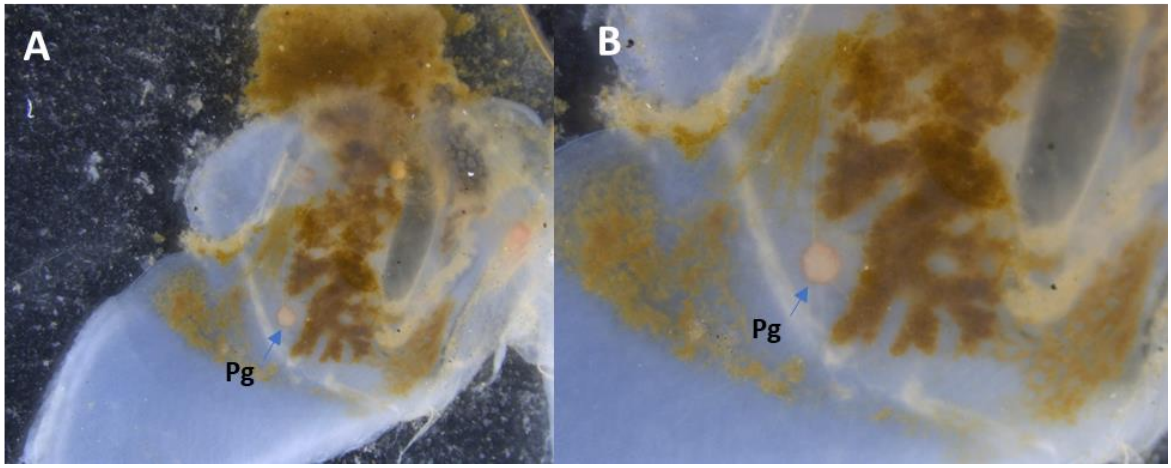

Figure 18 – *A. crassa* specimen squeezed between glass slide and cover slip, observed under stereomicroscope: (A) and (B) show the location of the pedal ganglion (Pg) in the foot.

Two statocysts were always present near the ganglia, each positioned to the sides of the bivalve (Figs. 17 and 19). Each statocyst is composed of a capsule made of a thin cellular layer, and in its interior a single spherical statolith is present. Each statocyst is clearly connected to the ganglia via nervous tissue, in a near symmetrical fashion. Details regarding the fine cellular structure of the statocyst were not determined. The type of statocyst-statolith system is concordant with the classification given by Morton of the type B1, generally described as a capsule consisting of an epithelium of several ciliated sensory cells containing a single spherical statolith inside.

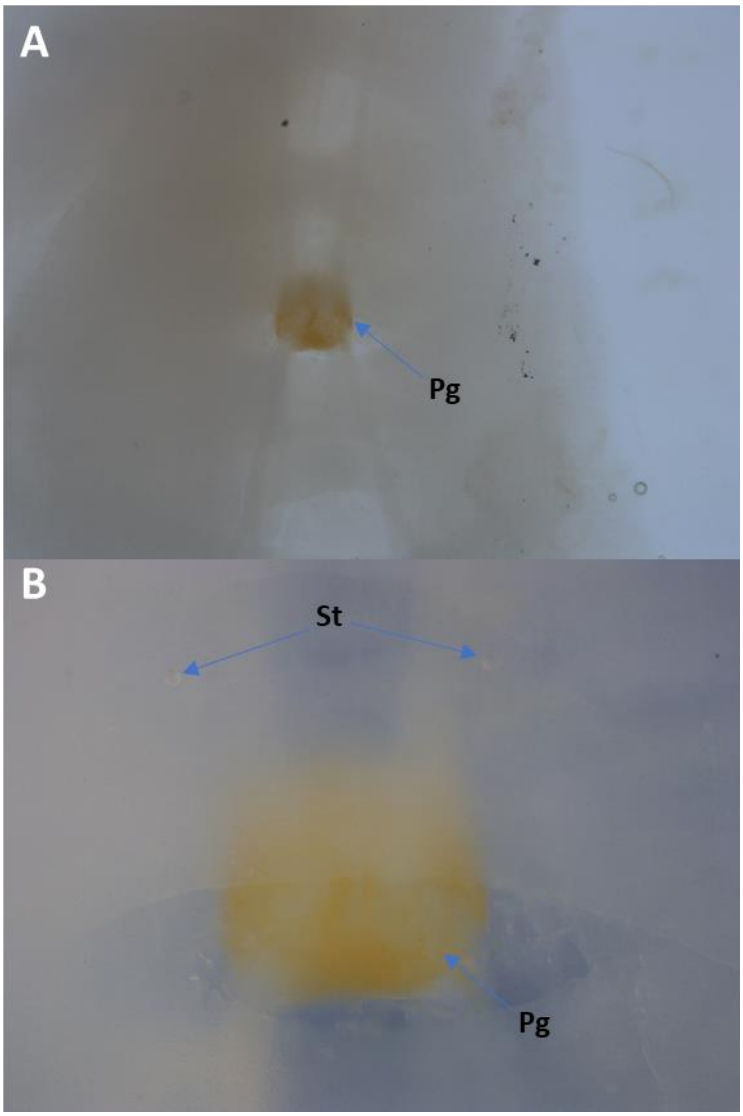

Figure 19 – Transversal cut of a small piece of tissue of the foot in *S. solida* containing the pedal ganglia after 30-60 min. digestion by immersion in a 1:1 mixture of 35% H_2O_2 and 0.1N NaOH in distilled water (see Fig. 12E in Materials and Methods). (A) Pedal ganglia (Pg); (B) Pair of statoliths (St).

Several attempts were made trying to find statoliths in both adults and juvenile specimens of *Mytilus galloprovincialis* and *Crassostrea gigas* of a variety of sizes (n= 20, SL from 5 to 30 mm), as well as in oyster larvae (pediveliger stage, approximately 17 days old obtained from an hatchery), but all attempts proved unsuccessful. In adult mussels, the statocyst is described to be of similar shape to those already found in this work, but no details are present on the nature of the statoparticles (Bayne, 1976). The only other description in the literature is on freshwater mussels of the genus *Unio*, who are described to have a single statolith inside the statocyst (Jordan & Verma, 1963), consistent with type B1 .

Nonetheless, the morphological type of statoliths present might differ in the case of marine mussels, perhaps statoconia being present instead, as is the case with types B2 and B3. No information detailing the statocysts in adult *C. gigas* specimens was found in the literature. However, in larvae of *Crassostrea virginica*, studies regarding responses to water flow changes have shown behavior consistent with possessing gravireceptor organs (Fuchs et al., 2015; Galtsoff, 1964). Oyster larvae exhibit a more complex nervous system than that present in adult oysters. In oyster larvae statocysts are said to be located near the pedal ganglia, both disappearing completely during metamorphosis (Harris, 1932; Galtsoff, 1964). Oysters are sessile after settlement, therefore possessing gravireceptor organs would be functionally unnecessary. It is conceivable that the structure does regress completely as an evolutionary adaptation. The size and structure of oyster larvae statocysts is unknown, as it is its precise time of formation. It is possible that the pediveliger larvae observed had not completely develop statocysts at the time, and consequently could not be found.

3.2 – Hydrological parameters in aquaculture

Hydrological parameters registered in the clam aquaculture nursery (03/11/2015 to 17/05/2016) are shown in Fig. 20 (Temperature in Fig. 20A, Dissolved Oxygen in Fig. 20B and Salinity in Fig. 20C). Water dissolved oxygen concentration (Fig. 20B) is only shown from 27/11/2015 onwards due to a malfunction of the equipment. Water temperature (Fig. 20A) ingrooved slightly in from early to mid-November, decreasing afterwards until the end of the month and stabilizing for the next four months. Only in early April 2016 did temperature started to rise again. In the months recorded, water temperature varied between 9.7 and 22.1 °C. Dissolved oxygen (Fig. 20B) varied from 4.9 to 11.3 mg/L, being generally lower during December 2015 and January 2016 (4.9 to 8.5 mg/L), increasing slightly and stabilizing from February to April 2016 (7 to 11.3 mg/L), decreasing again at the end of the month and showing high variability in March 2016 (5.1 to 9.6 mg/L). Water salinity varied from 21 to 35 ‰ (Fig. 20C). Salinity values remained stable, over 30 ‰, from early November until 21 December, decreasing afterwards and remaining around 25‰ for the remaining months. Temperature, salinity and dissolved oxygen values recorded are within acceptable range for *R. decussatus* development (Bayne, 1976; Sobral & Widdows, 1997; Jara-Jara et al., 1997). Nonetheless, slow growth rates are expected during winter months for bivalve species due to low temperatures (Moss et al., 2016). Since sampling of *R. decussatus* occurred during winter months, where growth is minimal due to low metabolic rate, statolith growth marks were not observed in specimens sampled in December and March 2016. Low salinity peaks

(<25‰) occurred in March and April, which are known to cause osmotic stress and negatively impact growth rate and increase mortality (Carregosa et al., 2014).

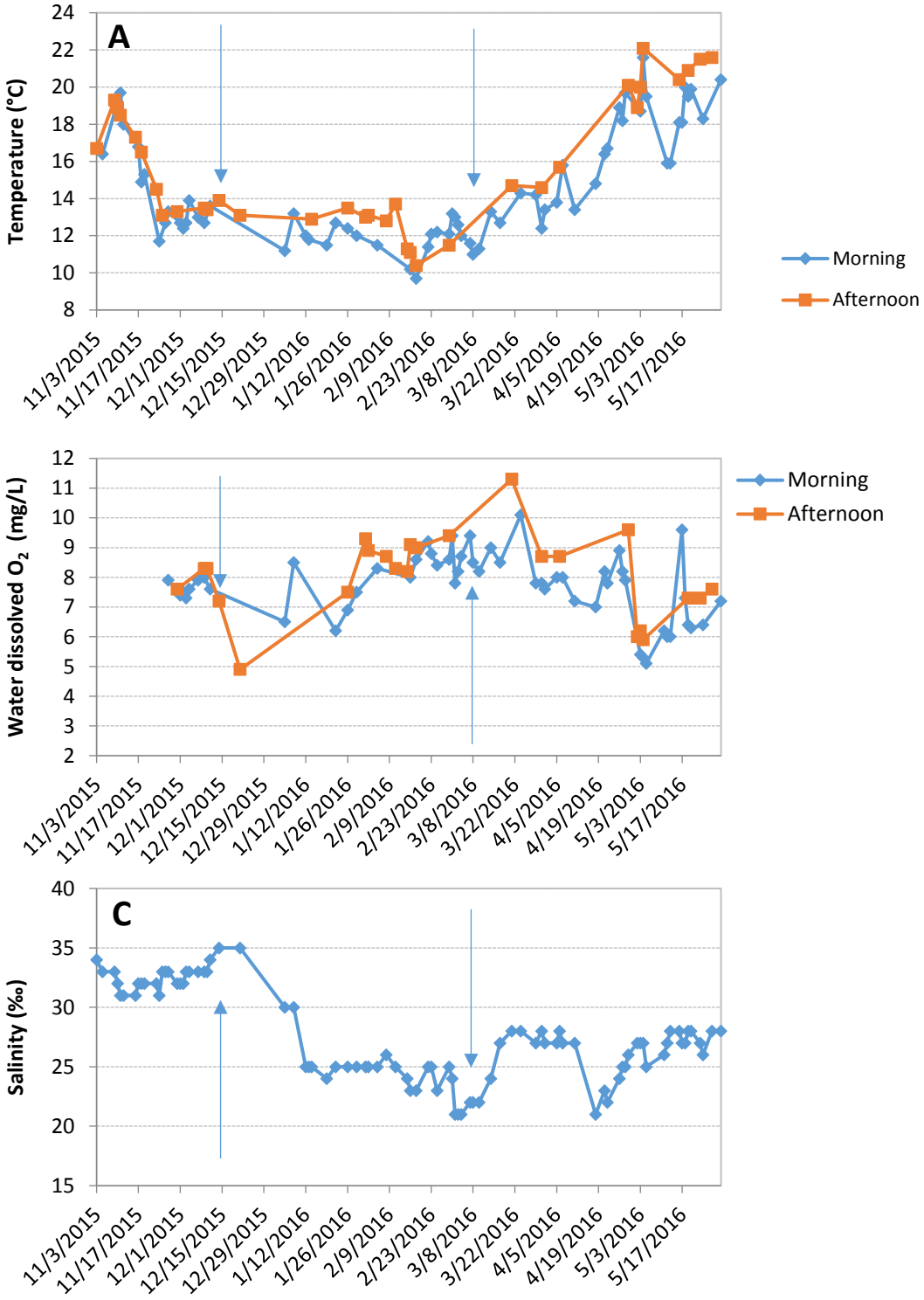

Figure 20 – Evolution of hydrological parameters (arrows mark dates of *R. decussatus* sampling): (A) Surface water temperature (°C), measured in the morning and afternoon; (B) Water dissolved oxygen, measured in the morning and afternoon (mg/L); (C) Water salinity (‰).

3.3 – Statolith microstructure

Morphologically, all the statoliths observed in the current study are sphere shaped, appearing to be crystalline in nature (Figs. 21 and 22). They are composed of a hard, yet extremely fragile substance. The statolith itself is very similar in shape to those already documented in several species of caenogastropods (Galante-Oliveira et al., 2013). Unlike in gastropods however, the bivalve statolith is much smaller. The largest statoliths found in this work belonged to the species *S. solida*. In specimens, approximately 4 years of age (4 shell growth marks), with average 40.99 ± 1.32 mm SL, statolith diameter (StD) corresponded to 62.7 ± 2.66 µm. In a study (Galante-Oliveira et al., 2013) on the statoliths of several different species of caenogastropods, the smallest sized statoliths found belonged to the species *Peringia ulvae*, where fully grown adults of average shell height (SH) 7.44±0.61 mm, presented statoliths with an average diameter of 41.2±2.6 µm. The largest gastropod statoliths documented by (Galante-Oliveira et al., 2013) were found in the species *Charonia lampas* (mean SH= 168.67 ± 39.46 mm, mean StD= 344.0 ± 39.9 µm). Although the statolith diameter is 8 x larger in *C. lampas*, the shell size is nearly 23 x larger than *P. ulvae*, which means that the relationship between statolith and shell size is not directly proportional.

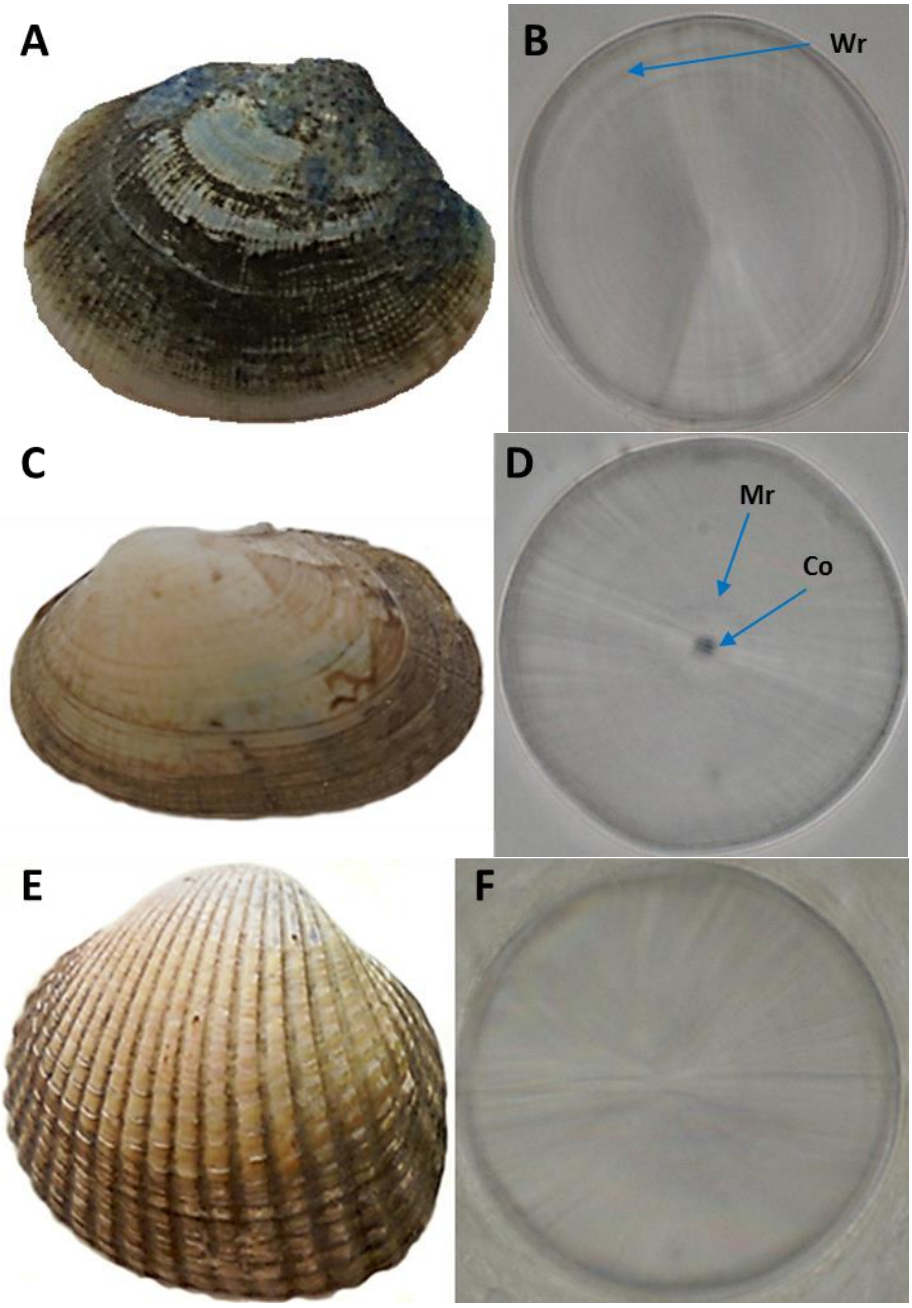

Figure 21 – Bivalve shells and corresponding statoliths observed under OM in 1000X magnification: *R. decussatus* (A) Shell SL = 12.46 mm; (B) Statolith StD = 32.9 µm. *V. corrugata* (C) Shell SL = 17.41 mm; (D) Statolith StD = 33.5 µm. *C. edule* (E) Shell SL = 20.54 mm; (F) Statolith StD = 36 µm). Mr = Metamorphic ring; Co = Statolith core; Wr = Winter ring.

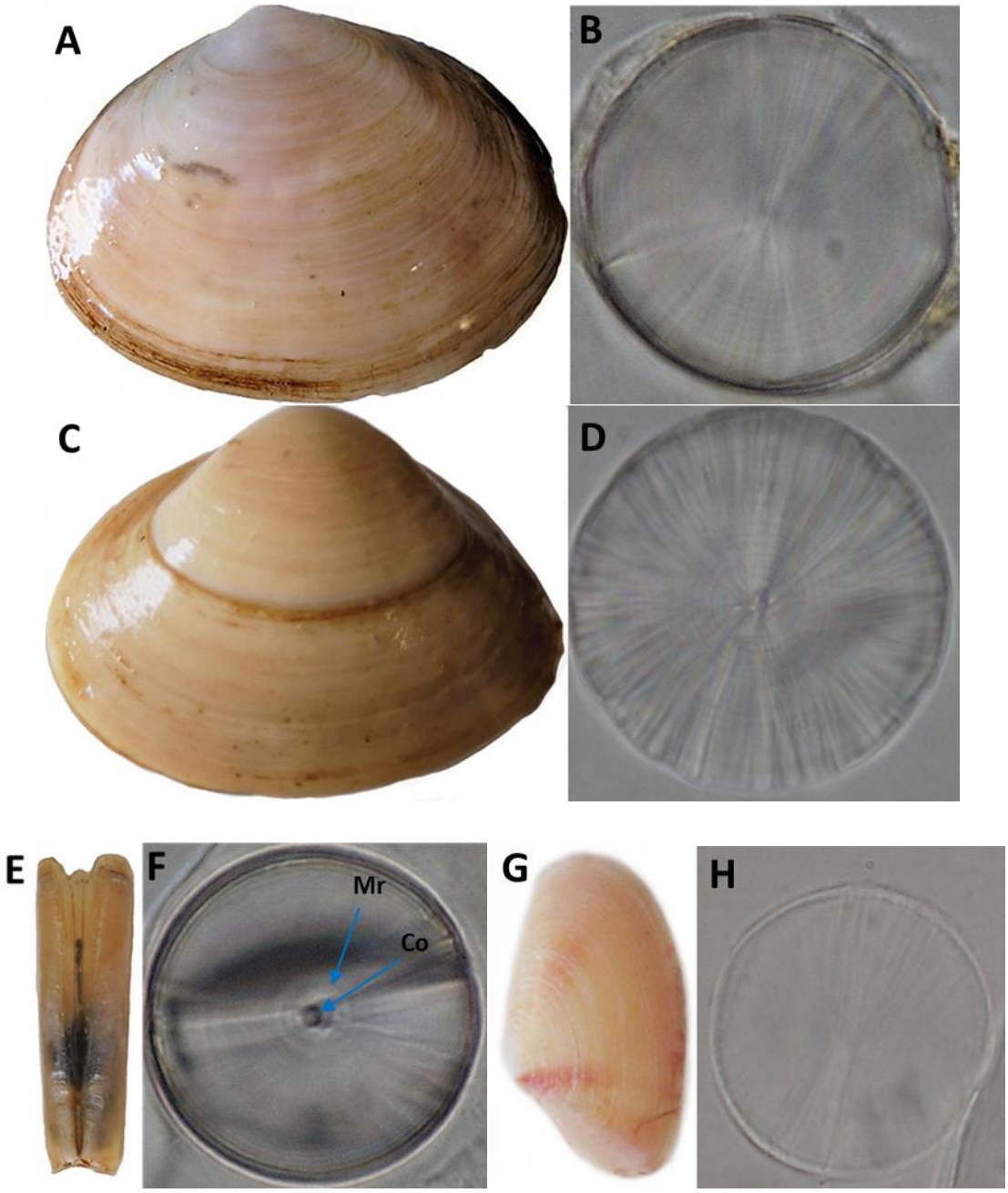

Figure 22 – Bivalve shells and corresponding statoliths observed under OM in 1000X magnification: *S. plana* (A) Shell SL = 42.92 mm; (B) Statolith StD = 35 µm. *S. solida* (C) Shell SL = 32.17 mm ; (D) Statolith StD = 48.1 µm. *S. marginatus* (E) Shell SL = 24.67 mm; (F) Statolith StD = 26 µm; *A. crassa* (G) Shell SL = 9.78 mm; (H) Statolith StD = 25.3 µm. Mr = Metamorphic ring; Co = Statolith core.

Paired statoliths of each specimen were very similar in shape and size in all species studied, with rare exceptions. Linear regressions of paired statoliths are shown in Fig. 23 for the species *R.*

decussatus, *V. corrugata*, *C. edule* and *S. plana*, since good number of statoliths were measured only in these species. Interestingly, in two specimens of *S. plana* and one of *V. corrugata*, the paired statoliths were particularly different in diameter, one being considerably larger than the other (Fig. 24).

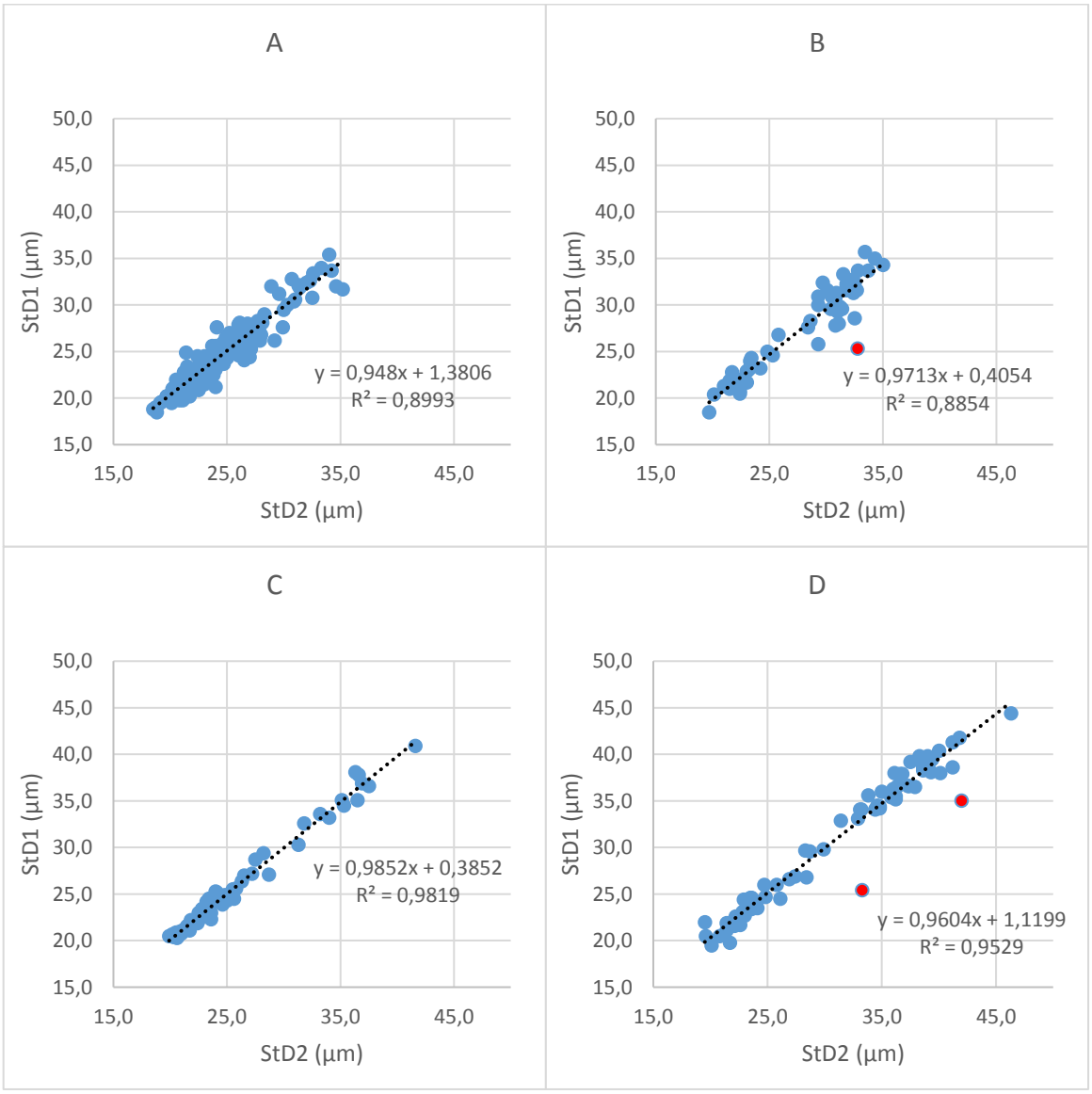

Figure 23 – Relation between paired statoliths: (A) *R. decussatus* (Dec_PT); (B) *V. corrugata*; (C) *C. edule*; (D) *S. plana*. Linear regressions are present, with respective equations and R^2 values given in each plot; red dots in plot are abnormally sized paired statoliths (see Fig. 24).

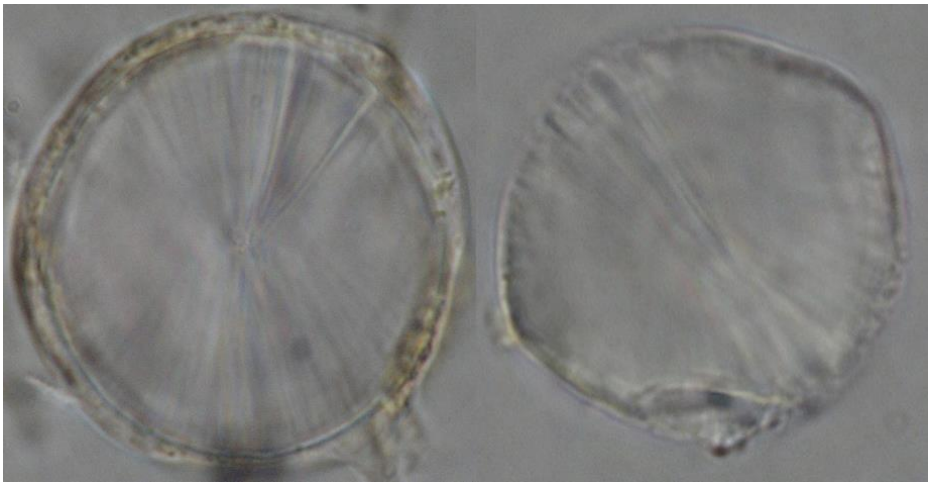

Figure 24 – Statolith pair of *S. plana* specimen, presenting high difference in StD: (Left) StD= 33.3 µm; (Right) StD=25.4 µm.

Most statoliths observed have a central nucleus or core (see Figs. 21 and 22), evident under OM, from which the structure seems to develop. Many concentric rings can then arise between the nucleus and the edge of the statolith, which result from additional increments of material as the animal grows. The first ring (when observable) is particularly intense (see Figs 21D, 22F and 13F in Material and Methods) common to the statoliths of most specimens analysed. As bivalves experience indirect development, this growth check is believed to correspond to a "metamorphic" ring (MR, Fig. 25C), similar to the established by Barroso and et al., (2005) for the first growth ring found in the statoliths of the gastropod species *Nasssarius reticulatus*, formed during the metamorphosis undergone by larvae prior to settlement, and then validated in other species of the same taxon sharing the same development type (Chatzinikolaou & Richardson, 2007; Galante-Oliveira et al., 2013). In *R. decussatus* (Dec_PT), the first ring has a diameter of approximately 6.74±0.96 µm. Several faint growth increments can be seen, immediately followed by a second strong ring of 12.87±0.78 µm in diameter. This strong ring observed in only 2 statoliths from 2 different specimens of the *R. decussatus* July 2016 sample (Fig. 25C).

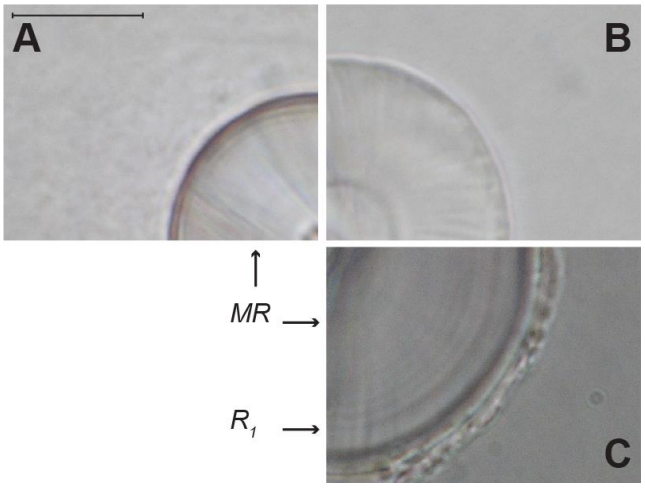

Figure 25 – *R. decussatus* (Dec_PT) statolith quarters from: (A) Specimen of SL = 4.47 mm (Dec.2015); (B) Specimen of SL = 13.22 mm (Mar.2016); (C) specimen of SL = 13.42 mm (July 2016). Arrows indicate visible check marks, possibly corresponding to the metamorphic ring (MR, common to all specimens analyzed), and the first winter ring (R1, visible in 2 specimens of the sample collected in July 2016). Scale bar in A is shared by all structures (A – C) and is equal to 10 µm.

Theoretically, and similarly to what has already been validated in many caenogastropods (Richardson et al., 2005; Galante-Oliveira et al., 2013; Galante-Oliveira et al., 2015; Hollyman et al., 2017), this strong growth mark may have been formed by the slower growth rate (or cessation) experienced during lower temperature months (from November 2015 to March 2016), corresponding to the first winter ring (R_1, Fig. 25C). Winter rings were not observed in specimens sampled in March 2016, likely due to the low temperatures still present (see Fig. 20A in Hydrological parameters in aquaculture), and growth rate still being slow. Winter rings are also formed in the shell, although several other factors can contribute to abnormally forming multiples rings per year, including stress factors such as the drop of salinity observed in March and April 2016 (see Fig. 20C in Hydrological parameters in aquaculture). Despite rings in the shells being present in most specimens at the time, a second strong ring in the statolith was observed only in 2 specimens. These were possibly the ones to have resumed growth faster after the temperature increase in Spring (from March on), already showing (in July) sufficient matrix deposition after the newly-formed ring, allowing its observation. As no further samples were obtained, we can only speculate that R_1 could have been deposited in all other specimens of the July 2016 *R. decussatus* (Dec_PT) sample, and that the calcification progress in the following (Summer) months could have allowed its observation. Should no other strong rings be formed until November 2016, a year would correspond to a single winter ring in the statolith. Age determination by the means of statolith ring analysis might be possible in this species, but more work needs to be done before this methodology can be validated.

In several of the other species studied, statolith rings could be observed as well (see Figs. 21 and 22), but the frequency of their formation differs, and direct correspondence between statolith rings vs growth period is difficult to establish.

In *V. corrugata*, sampling first occurred in April 2016, then later in September. As such, specimens observed were very young, not having gone through a full winter-summer cycle. No rings beyond the metamorphic ring were observed in clams pertaining to this sampling. Older specimens (n = 3) were procured from an earlier aquaculture development cycle. Specimens were at least a year old, having marked a winter ring in the shell, although the precise age is unknown. These specimens, having already gone through at least a winter-summer cycle, several rings were observable in the statolith (Fig. 21C and D), although faintly. A correspondence between statolith ring and age of the clam is, therefore, hard to establish for this species based on the results obtained.

Similarly, *A. crassa* specimens studied were of small sizes (SL< 10 mm), and no rings were marked in the statolith. Potential for age determination using the statolith is unclear in this species.

In *C. edule*, statolith rings were mostly absent, even the metamorphic ring is very faint and difficult to see. The opposite occurs on *S. plana*. In this species, statoliths show a large number of rings, too many for a direct correspondence with marks on the shell. This suggests that multiple rings are formed per year. Rings are also extremely alike, having similar intensity and possess no other apparent distinction between them. At this point, potential usage of statolith rings as tools for age determination is limited in both of these species, although for different reasons.

In *S. solida*, many rings are also present in the statolith, indicating the formation of several rings per year as well. Unlike in *S. plana* however, some rings seem to be slightly stronger than others, but not as apparent as in *R. decussatus*. Shell rings are considered a very good age determining tool in this species since each ring is clearly defined and only one is (usually) formed per year(Gaspar et al., 1995). A direct correspondence between shell rings and statolith rings is hard to make based on the results obtained.

Improvements to the methodology used could definitely provide more information in some cases.

Although only explored in *R. decussatus*, the periodicity of all statolith increments can be studied. This would be of particularly importance in *S. plana* and *S. solida*, since rings possess little distinguishable features from each other. Since in these species a single annual ring is perhaps absent, knowing the time necessary for each ring to be formed is essential.

Due to the statoliths' spherical shape and the incremental formation of the growth marks, optical interferences can be misinterpreted as additional rings. In molluscan statolith studies, it is common practice to embed the entire structure in resin, then grind and polish until reaching the middle

plane. This allows for a much clearer view of all statolith rings and minimises any optical interferences that might occur. Unfortunately, due to the miniscule size and frailty of the bivalve statolith, efforts to directly apply this methodology were unsuccessful.

3.4 – Statolith diameter (StD) and shell length (SL) relationships

Relationships between shell length (SL) and statolith diameter (StD) for the species *R. decussatus* (Dec_PT and Dec_H), *V. corrugata*, *C. edule* and *S. plana* are shown in Fig. 26. Relationships in *R. decussatus* were made for each breeder batch (Dec_PT in Fig. 26A and Dec_H in Fig. 26B) separately. *R. decussatus* specimens collected in December 2015 and March 2016 are shown in orange, while sampling in July is shown in green (Fig. 26A only). Regressions in *R. decussatus* (Fig. 26A - Dec_PT: $y=0.0005x^{3.0678}$, $R^2=0.7727$; Fig. 26B - Dec_H: $y=0.0002x^{3.2721}$, $R^2=0.8444$), *V. corrugata* (Fig. 26C: $y=7E\text{-}05x^{3,4958}$, $R^2 = 0,88$) and *S. plana* (Fig. 26E: $y = 0,0002x^{3,3737}$, $R^2 = 0,9496$) are best described as power functions, while results for *C. edule* (Fig. 26D: $y=39,709\ln(x) – 115.38$, $R^2= 0,8869$) best fit a logarithmic regression. As observed in Fig. 27, StD growth accompanies SL growth, but expected StD at a given SL varies for each species, suggesting that statolith growth accompanies the growth of the specimens through their life-cycle, and is specific for each species. Regressions for Dec_PT (Fig. 26A) and Dec_H (Fig. 26B) corresponding to the sampling periods of December 2015 and March 2016 show values of $R^2=0.6909$ and $R^2=0.8444$, respectively. Studies performed by Barroso et al., (2005) and Galante-Oliveira et al., (2013) on the relationship between shell height vs statolith diameter in the gastropod species *Nassarius reticulatus* and *Nucella lapillus* achieved results similar to those obtained here. In these studies, relationships were observed, although presented a different trend, and found to be specific to each species and population/sampling site.

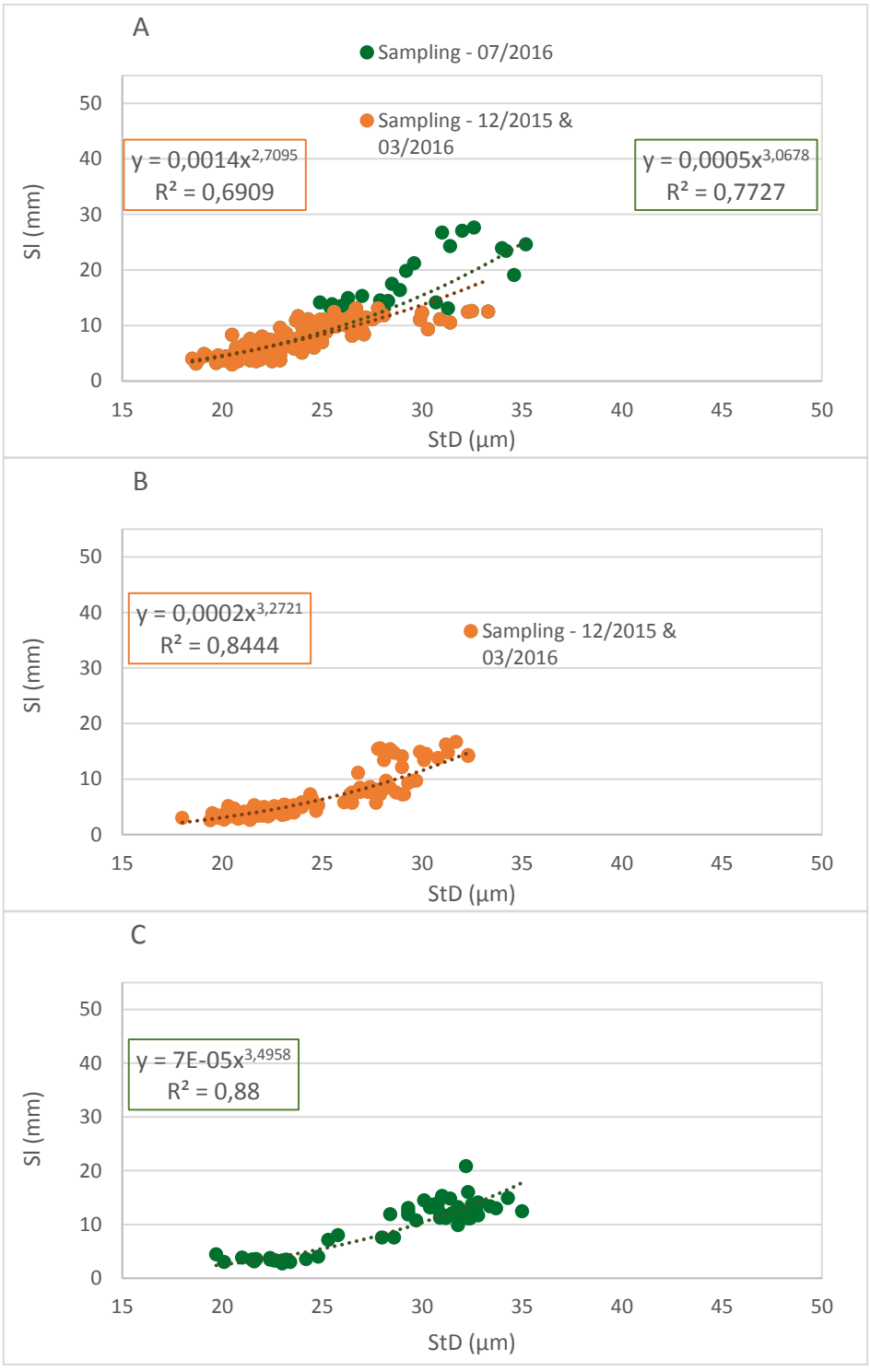
A
Sampling - 07/2016
Sampling - 12/2015 & 03/2016
y = 0,0014x^2,7095
R² = 0,6909
y = 0,0005x^3,0678
R² = 0,7727
SI (mm)
StD (µm)
B
y = 0,0002x^3,2721
R² = 0,8444
Sampling - 12/2015 & 03/2016
SI (mm)
StD (µm)
C
y = 7E-05x^3,4958
R² = 0,88
SI (mm)
StD (µm)

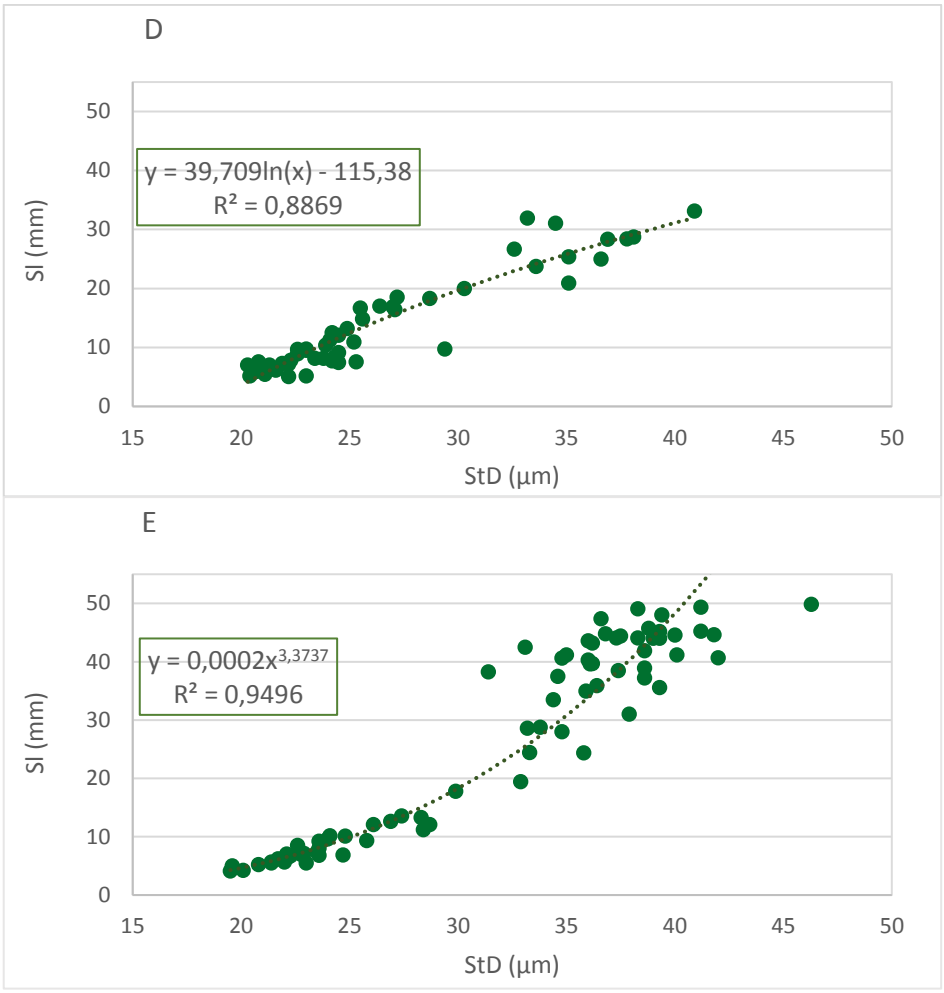

Figure 26 – Relationship between shell length (SL) and statolith diameter (StD) in *R. decussatus* (Dec_PT=A; Dec_H=B), *V. corrugata* (C), *C. edule* (D) and *S. plana* (E). Power regressions are shown in A, B, C and E, while a logarithmic regression is shown in D. Regression equations and coefficient of determination are shown in each plot.

3.4 – Electron Microprobe Analysis

Energy dispersive x-ray spectra (EDS) performed on *R. decussatus* (Dec_PT) statoliths reveals Ca, O and C as major elements in the statolith composition. Etched statoliths showed signs of effervescence (Fig. 27), suggesting a basophilic nature. An expected result, in accordance with previous work done on statolith elemental analysis in gastropod and cephalopod species (Galante-Oliveira et al., 2014; Radtke, 1983). Since no quantification of elements was done, precise concentration of the main elements is not known. Several minor elements were detected as well, including Si, S, Na and Cl (Fig. 28). Cl was only detected in etched statoliths, most likely a remnant of the acid used for the etching that was not fully removed by washing. Secondary electrons image (SEI) of an intact statolith reveals an overall spherical form, with a relatively smooth surface area with several small grooves (Fig. 29). Whether these grooves are a natural occurrence or caused by damage incurred due to the handling of the statoliths is uncertain. SEI image of a statolith fractured on the middle plane (Fig. 30 A and B) shows what are possibly very faint growth rings. In particular, one ring is perceptible. Based on the results obtained for *R. decussatus* in OM, this ring should neither be a winter ring nor a metamorphic ring. A winter ring would be positioned closer to the periphery of the statolith and a metamorphic ring closer to the center. As the fracture plane is extremely rugged, particularly in the central area of the statolith, finer details are possibly masked, such as the expected metamorphic ring. Moreover, and contrary to what has been observed in gastropod statoliths (Galante-Oliveira et al., 2014), no preferential formation axis or crystal orientation marks are observable. Back scattered electrons image (Fig. 30 C and D) reveals the growth ring in a lighter tone when compared to the surrounding area, suggesting that heavier elements are present in the ring. EDS analysis on the ring reveals a particularly great amount of calcium, but an unexpected drop in oxygen and carbon concentrations because growth rings are claimed to be rich in organic matrix. No other elements were present in any meaningful concentration. Since calcium is heavier than both oxygen and carbon, a proportionally higher concentration of calcium in the ring can result in a lighter tone in a BSE image. Additionally, a possible ring is detectable in the extreme periphery of the statolith (Fig. 30 C and D). A ring in this is position is consistent with a winter ring, since the specimen would have formed the ring very recently. This is different from what has been observed previously in gastropod statoliths. In gastropods, statolith growth rings are very well marked and are easily observable. Furthermore, EDS images show the rings in a darker tone when compared to the remaining matrix, suggesting comparatively lighter elements being predominant.

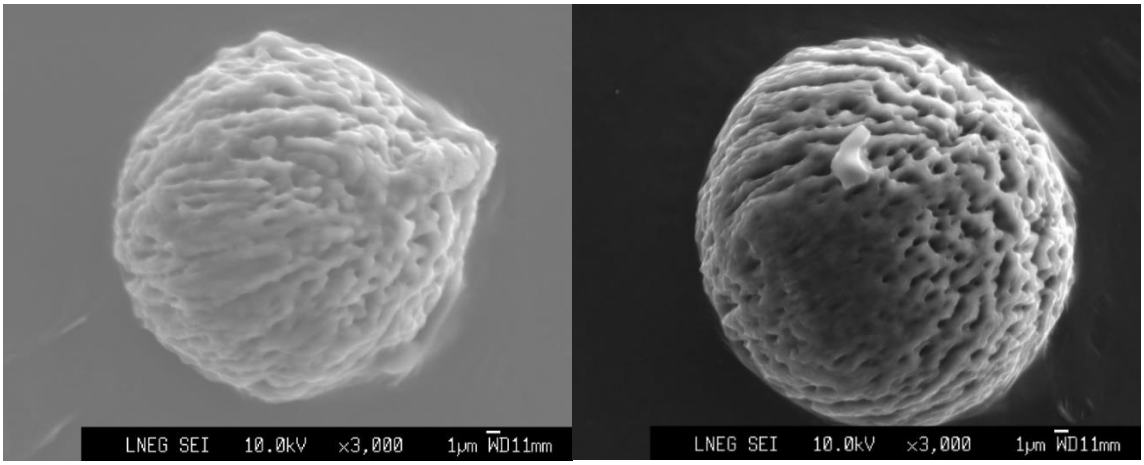

Figure 27 – Secondary electrons image (SEI) of two different *R. decussatus* (Dec_Pt) statoliths etched by HCl (0.1M) for approximately 30 to 40s.

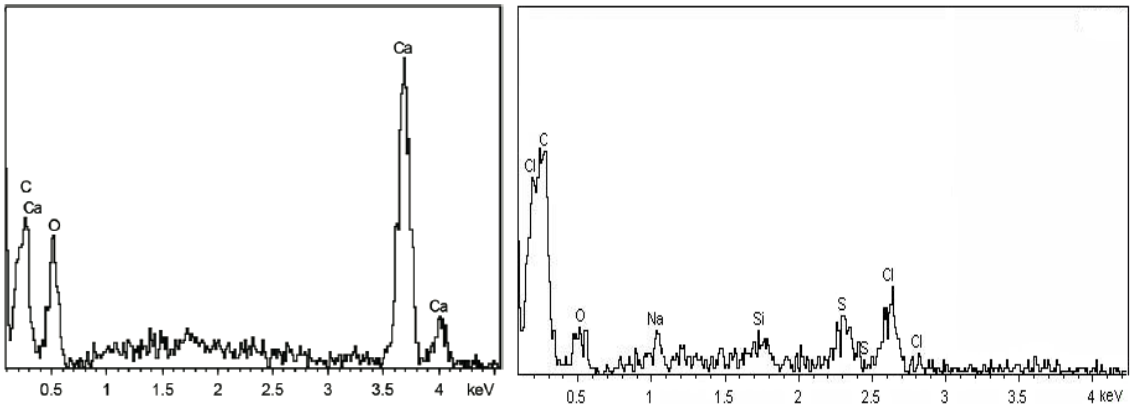

Figure 28 - EDS spectra of *R. decussatus* (Dec_Pt) statoliths: (Left) spectra acquired on the fracture plane of a statolith, showing X-ray lines for Ca, O and C; (Right) spectra acquired on the surface of a statolith etched by HCl (0.1M), showing X-raylines for Cl, as well as for several other minor elements (Na, S, Si).

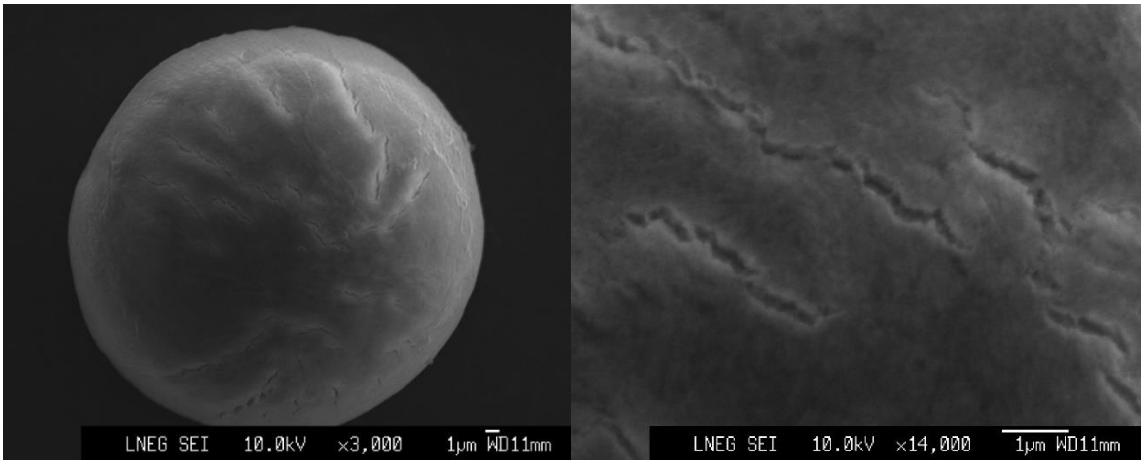

Figure 29 – Microanalysis of *R. decussatus* (Dec_PT) statolith: (Left) Secondary electrons image (SEI) of an intact statolith; (Right) Higher magnification of the small grooves on the statoliths' surface.

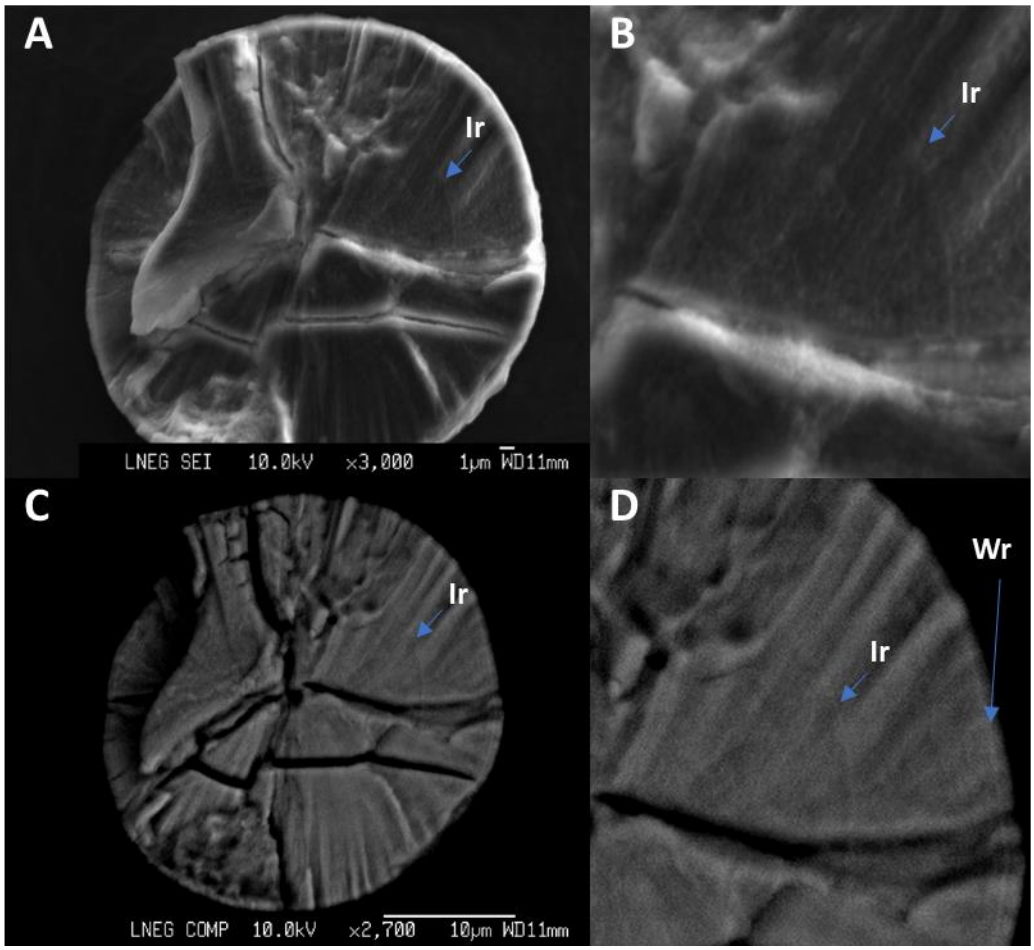

Figure 30 – Microanalysis of a fractured *R. decussatus* (Dec_PT) statolith: (A) and (B) Secondary electrons images (SEI) of fractured statolith showing a possible interference ring (Ir); (C) and (D) Back scattered electrons image (BSE/COMP) of fractured statolith showing a possible interference ring (Ir) and a possible winter ring (Wr).

3.5 – Micro-Raman Spectroscopy

Micro-Raman spectra acquired in *R. decussatus* (Dec_PT) statoliths are shown in Figs. 31 and 32. Two distinct minerals were detected: amorphous calcium carbonate (in Fig. 31) and crystalline calcium oxalate (in Fig. 32).

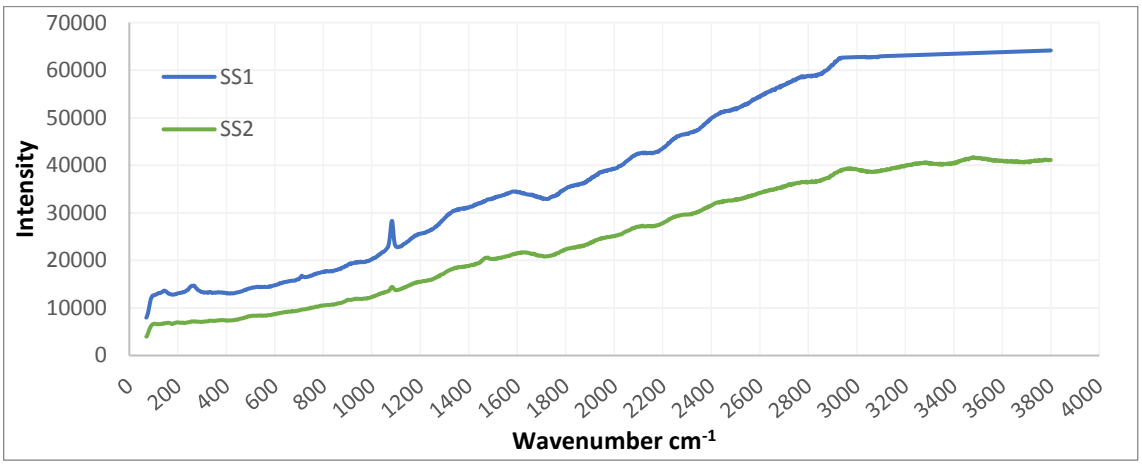

Figure 31 – Raman spectra acquired between 70 and 3800 cm^{-1} in a smashed statolith at two different locations (SS1 and SS2; to see the location where spectra were acquired see Fig. 14 in the Materials and Methods section) suggesting the presence of calcium carbonate within the matrix.

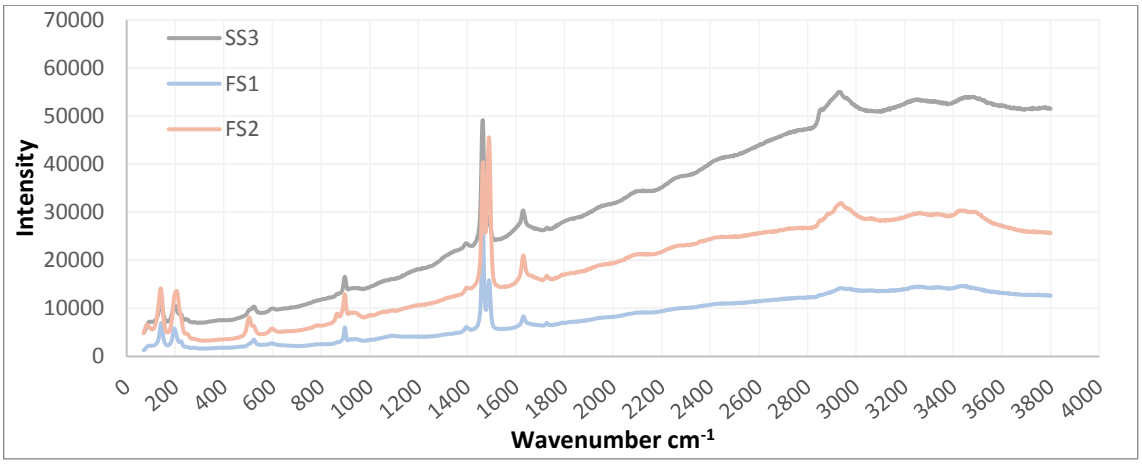

Figure 32 – Raman spectra acquired between 70 and 3800 cm^{-1} on both smashed (SS3) and fractured statoliths (FS1 – centre of the statolith; FS2 – periphery of the statolith; to see the location where spectra were acquired see Fig. 14 in the Material and Methods section), suggesting the presence of calcium oxalate within the matrix.

Regarding the first, the SS1-spectrum acquired in a smashed statolith (blue line in Fig.31) match the presented by Wehrmeister et al. (2011) for the amorphous phase of a biogenic carbonate (Fig. 33).

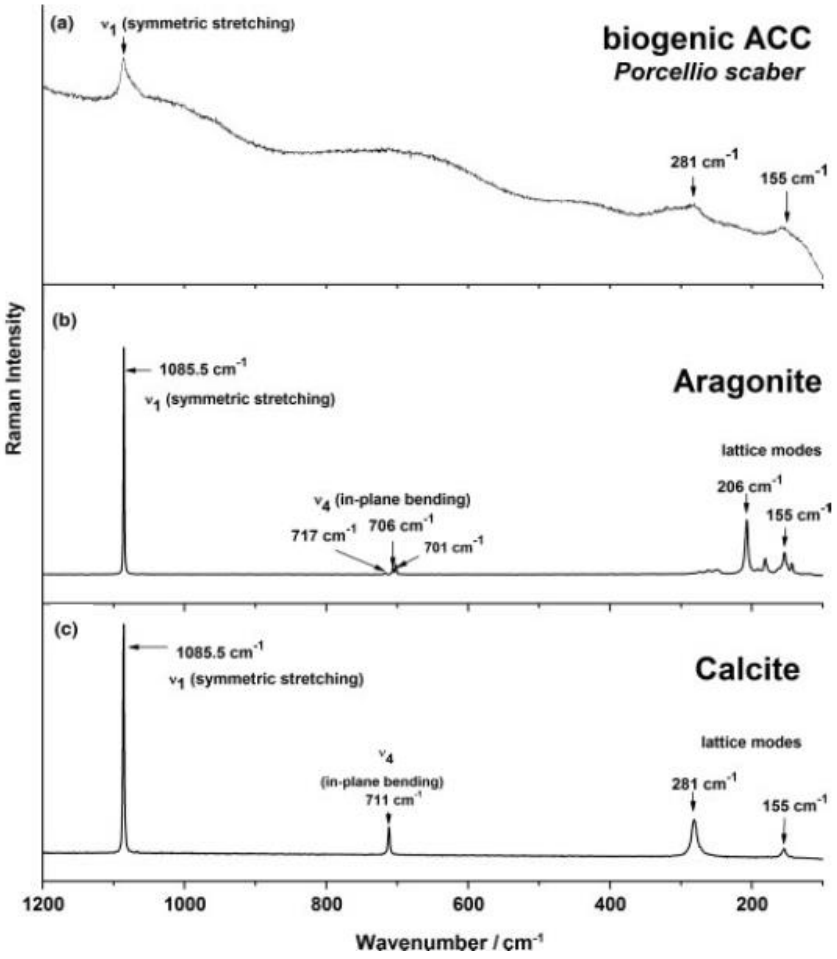

Figure 33 – Raman spectra of: (a) biogenic amorphous calcium carbonate in *Porcellio scaber*; (b) standard Raman spectra of aragonite; (c) standard Raman spectra of calcite. Extracted from Wehrmeister et al. (2011).

Contrasting with the sharp peaks characteristic of crystalline polymorphs, the broad and lower energy peaks observed in the SS1-spectrum in Fig. 31 are typical of an amorphous phase. This spectrum shows two broad peaks in the lattice mode region (at 148 and 267 cm^{-1}) that are characteristic of the calcium ion, and two sharper peaks at 715 cm^{-1} and 1085 cm^{-1}, the first lower in energy, matching the in-plane bending mode $\nu 4$ and the symmetric stretching mode $\nu 1$ of the carbonate ion.

An overall different molecular structure is disclosed by the spectra in Fig. 32 that match the presented by Conti et al. (2015) for calcium oxalate (Figs. 34 and 35).

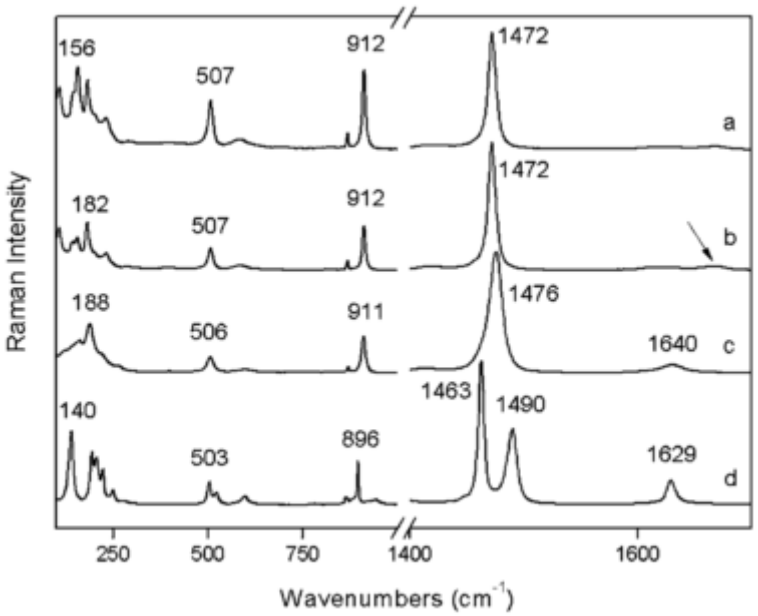

Figure 34 – Raman spectra between ≈125 and ≈1700 cm^{-1} of the three calcium oxalate hydrated forms: (a) trihydrated, COT (785 nm laser); (b) COT (532 nm laser); (c) dihydrated, COD (532 nm laser); (d) monohydrated, COM (532 nm laser). Extracted from Conti et al. (2015).

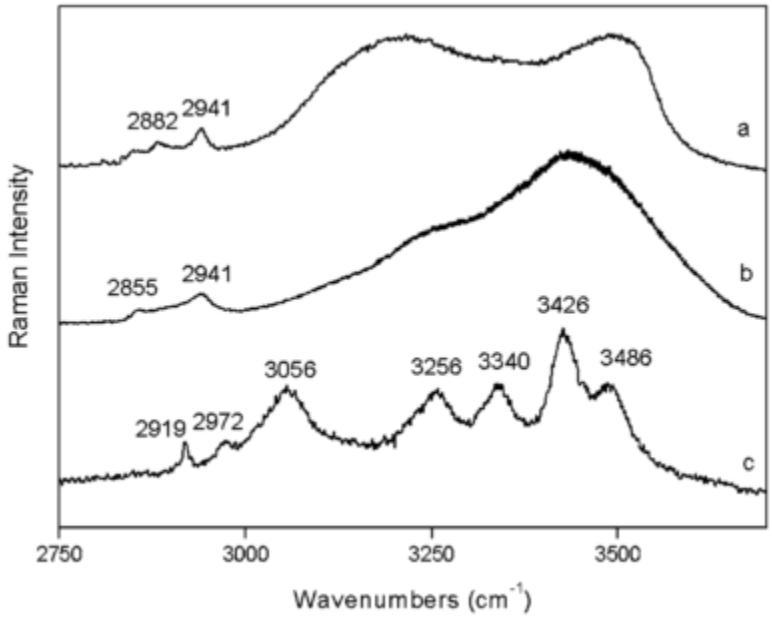

Figure 35 – Raman spectra between 2750 and ≈3750 cm^{-1} of the three calcium oxalate hydration forms with a 532nm laser: (a) trihydrated (COT); (b) dihydrated (COD); (c) monohydrated (COM). Extracted from Conti *et al.* (2015).

At first, when compared with the SS1-spectrum in Fig. 31, the sharper peaks seen in Fig. 32 suggest higher crystallinity of those statoliths' matrix. Additionally, spectra in Fig. 32 show bands in the 130 to 250 cm^{-1} region that are consistent with the Ca-O bond stretching and bending vibrations; peaks between 500 and 600 cm^{-1} that can be attributed to the O-C-O group bending, followed by the C-C stretching between 850 and 950 cm^{-1}; larger peaks in the region from 1400 to 1500 cm^{-1} which are characteristic of the symmetric C-O stretching, followed by the antisymmetric C-O stretching signal between 1630 and 1735 cm^{-1} (Hug et al., 2012). Noteworthy that a blank spectrum (i.e., acquired from the silicon glass slide where samples were placed for the analysis) was not assessed and not subtracted from the ones of our samples, reason why exact peak positions might be slightly shifted from their reference values. Even though, the peaks identified in our spectra in Fig. 32 are all correspondent to the signals described for calcium oxalate (Conti et al., 2015); exception made to the slight elevation observed at the 1100 cm^{-1} region in spectrum FS1 (Fig.32) that, as reported by Hajir et al. (2014), can be attributed to a trace of ethanol used to clean structures prior to spectra acquisition.

Calcium oxalate is found in three different forms, depending on the degree of the molecule hydration (Hajir et al., 2014). The more stable, and most commonly found, is the calcium oxalate monohydrated (COM), followed by a less common dihydrated (COD) form, and the much rarer, unstable, calcium oxalate trihydrated (COT). Raman spectroscopy allows the distinction between these three forms as showed in Figs. 34 (region between ≈125 and ≈1700 cm^{-1}) and 35 (between 2750 and ≈3750 cm^{-1}): COM shows bands at 246, 603 and 1721 cm^{-1}; the 508, 526, and then 868, 902 and 937 cm^{-1} bands in COM appear as a single peak in COD (Edwards et al., 1992); COT lacks the peak in the 1630 cm^{-1} region (Conti et al., 2015). In addition, the hydroxyl (OH) groups show characteristic stretching bands from 3000 to 3500 cm^{-1}, distinct for each hydrated form (see Fig. 35). COM presents several small peaks from 2919 to 3489 cm^{-1}; COD and COT have both larger elevations in this region, COT having two bands from the 3100 to 3500 cm^{-1}, and COD only one (Fig. 35). The bands shown in the far end of our spectra (Fig. 32) between 3000 and 3500 cm^{-1} are too vague and unclear to give concrete details regarding -OH groups characteristics, making hydrated form distinction not possible by this region. Nevertheless, spectra in Fig. 32 show Raman shift pattern with several peaks of both COM and COD, suggesting the presence of both forms in the statolith matrix, while the COT seems to be absent.

Our data are somehow distinct from what was expected since the presence of calcium oxalate has never been mentioned as being part of molluscan statoliths, which composition has always been referred to be calcium carbonate based, differing only in that mineral crystalline polymorph

(calcite, aragonite, vaterite). Biogenic calcium oxalate occurs naturally in several groups (plants, fungi, insects, and mammals; Campbell, 2017). In plants, it is particularly abundant in cacti (Frausto-Reyes et al., 2014), where it can correspond to almost 85% of a plant dry weight (Baran, 2015). It is present in many different plant tissues (e.g., roots, leaves, stems, seeds) in all hydrated forms. Functionally, it is involved in calcium regulation or storage, light reflection, mechanical support, detoxification, intracellular pH, and ion regulation (Campbell, 2017). In mammals, it is usually associated with pathological conditions as, for instance, as a constituent of human kidney stones (Bak et al., 2000). In bivalves, and to our best knowledge, the only record of its presence is in the kidney granules of *Pecten maximus* (Overnell, 1981), being this work the first report of this mineral in statoliths.

Finally, as described for biogenic mineral materials, namely in gastropod statoliths (Galante-Oliveira et al., 2014), the broad band of low energy clearly observed in Fig. 32 spectra between 2800 to 3000 cm^{-1} is characteristic of -CH functional groups and indicative of the presence of an organic matrix (Nehrke & Nouet, 2011).

Chapter 4 – General conclusions and future work

Analysis of the results obtained on the course of this study of bivalve statoliths in these species, have shown several interesting results, which are briefly summarized in this chapter.

Bivalve statocysts are located near the pedal ganglia, in the foot of the specimen. This was consistent among species studied. There are two statocysts per animal, each containing a single statolith. Statocysts and statoliths observed appear to be type B1 according to Morton (Morton, 1985). Morphologically, the statolith is a spherical mass composed of a translucent, hard yet fragile, material. A central nucleus is present and usually visible. Growth rings are often present as well. In some cases, a strong first ring is visible around the nucleus. In other groups, namely gastropods, the formation of this growth mark in the statolith is attributed to the metamorphosis of the animal, at the end of the larval stages, a process by which bivalves also go through. The resulting mark is what is called a metamorphic ring. The general microstructure of the bivalve statolith observed is very similar to those documented in several species of caenogastropods (Galante-Oliveira et al., 2013; Barroso et al., 2005).

In general, no obvious differences were found between the diameter of paired statoliths. The positive correlation between SL and StD in *R. decussatus*, *V. corrugata*, *C. edule* and *S. plana*, indicates that the statolith accompanies growth rate of the shell during the bivalve's lifespan. In the future, this type of work should strive to include as many species as possible, from larvae to matured adults. Regressions found in this work best fit a power function, with the exception of *C. edule* in which a logarithmic regression is present, but inclusion of data relating to the larval stage could reveal a different result, as shown for *N. reticulatus* in the works of Galante-Oliveira et al., (2013), Barroso et al., (2005) and Chatzinikolaou and Richardson (2007). Moreover, these regressions are species specific, indicating that for validation, this work must be done for each species.

The seasonal variation of the metabolic rate in bivalves in temperate waters leads to the formation of annual growth rings in the shell. In bivalves, the statolith growth is synchronized with the growth of the shell, and should statolith rings be formed at the same rate and pattern, age determination can be made by counting growth rings in the statolith too. In *R. decussatus* specimens, whose statolith growth was followed from December 2015 to July 2016, a correspondence could be made between the formation of a ring in the shell and a ring in the

statolith. Some further faint rings were observed, formed after the metamorphic ring, possibly caused by environmental stress factors that had an impact in the growth rate of the specimens. Should no other equivalent strong rings be formed until later that year, a single shell ring would correspond to an obvious strong ring in the statolith. As such, age determination by means of statolith ring analysis would be possible in this species. Nonetheless, for complete validation of this method for *R. decussatus*, additional work must be done, particularly in older specimens. In other species studied, however, statoliths rings were present but the frequency of their formation differs, and direct correspondence between these rings and annual growth seasonality is difficult to establish. This is particularly evident in *S. solida* where shell rings are established as reliable age determining tools (Gaspar et al., 1995), each ring in the shell corresponding to a winter-summer cycle (one per year). The rings registered in *S. solida* shells are outnumbered by those present in the statolith, which implies the formation of several rings per year in the statoliths. Hence, a more detailed analysis on statolith growth, as was done for *R. decussatus*, should be extended to more species. Sampling of specimens, ideally from as early in the lifecycle as possible, in a controlled environment, such as an aquaculture production or lab setting, might provide insight on periodicity of ring formation and possibly correlate the occurrence of adverse hydrological conditions with stress marks in the statolith.

Since statoliths are spherical and present several rings, optical interferences might have contributed to the difficulty in correctly counting the number of rings, giving the illusion of the presence of more rings than those present. Embedding the whole structure in resin, grinding and polishing to reach the statoliths' middle plane would have diminished the effect, and possibly allow to distinguish rings based on intensity. However, due to the small size of the statoliths, such efforts proved unsuccessful. Other methodologies to provide increased detail in the observation of bivalve statoliths should be explored in the future, to allow a better identification of rings.

Attempts to study the statoliths of the species *Mytilus galloprovincialis* and *Crassostrea gigas* were fruitless. Although mussel statocysts are described in adult specimens of this species (Bayne, 1976), none was found, and as far as we know, statolith morphology is not described in the literature for this species. Failure to locate statoliths in this species can be eventually attributed to the absence of statoliths or the existence of a different type of statoparticles, such as statoconia. However, freshwater mussels of the genus *Unio* are said to possess statoliths similar in structure to type B1 (Jordan & Verma, 1963). Whether marine mussels present the same type of statolith as their freshwater counterparts is something that should be investigated in future work. In *C. gigas* no information on statocysts in adult specimens was found. Oyster larvae, however, are said to

possess statocysts (Fuchs et al., 2015) that regress completely during metamorphosis (Harris, 1932). Although statocysts in oyster pediveliger larvae should already be formed, none was found in the ones examined in the current study.

Electron microprobe analysis of *R. decussatus* statoliths revealed that Calcium, Carbon and Oxygen are the primary elements, as it happens in cephalopod and gastropod statoliths (Rodhouse & Hatfield, 1990; Galante-Oliveira et al., 2014), suggesting a calcium carbonate matrix. BSE image of a fractured statolith reveals the growth ring in a lighter tone when compared to the surrounding area, suggesting that heavier elements are present in rings. EDS analysis on the ring reveals a particularly great amount of calcium, but an unexpected drop in oxygen and carbon concentrations since growth rings are claimed to be rich in organic matrix. However, Micro-Raman spectra acquisition points to a primary composition based on calcium oxalate, with a very slight presence of amorphous calcium carbonate. Of the three different hydration forms of calcium oxalate (mono, di and trihydrated), both the mono and dihydrated forms appear to be present in *R. decussatus* statoliths, while the trihydrated form is absent. Presence of calcium oxalate has never been mentioned as being part of molluscan statoliths. Even though biogenic calcium oxalate occurs naturally in several groups (plants, fungi, insects, and mammals; Campbell, 2017), the only record of its presence in bivalves is in the kidney granules of *Pecten maximus* (Overnell, 1981), being this work the first reporting this mineral in statoliths. Efforts to perform this type of elemental analysis in a wider range of bivalve species are necessary, since expected results obtained in other molluscan statoliths (elemental composition) might not apply for bivalves.

The results obtained in this study are, in essence, preliminary. The main challenge so far has been the extremely small size and fragility of the bivalve statolith. Nonetheless, potential for sclerochronology exists and should be explored in future studies.

Chapter 5 – Bibliography

Álvarez-Padilla, F., & Hormiga, G. (2007). A Protocol For Digesting Internal Soft Tissues And Mounting Spiders For Scanning Electron Microscopy. *Journal of Arachnology*, *35*(3), 538–542. https://doi.org/10.1636/Sh06-55.1

Arkhipkin, A., Argüelles, J., Shcherbich, Z., & Yamashiro, C. (2015). Ambient temperature influences adult size and life span in jumbo squid (*Dosidicus gigas*). *Canadian Journal of Fisheries and Aquatic Sciences*, *72*(3), 400–409. https://doi.org/10.1139/cjfas-2014-0386

Arkhipkin, A. I. (2005). Statoliths as "black boxes" (life recorders) in squid. In *Marine and Freshwater Research* (Vol. 56, pp. 573–583). https://doi.org/10.1071/MF04158

Arkhipkin, A. I., & Middleton, D. A. J. (2003). In-situ monitoring of the duration of embryonic development in the squid Loligo gahi (Cephalopoda: Loliginidae) on the Falkland shelf. *Journal of Molluscan Studies*, *69*(2), 123–133. https://doi.org/10.1093/mollus/69.2.123

Arkhipkin, A. I., & Shcherbich, Z. N. (2012). Thirty years' progress in age determination of squid using statoliths. *Journal of the Marine Biological Association of the United Kingdom*, *92*(6), 1389–1398. https://doi.org/10.1017/S0025315411001585

Bak, M., Thomsen, J. K., Jakobsen, H. J., Petersen, S. E., Petersen, T. E., & Nielsen, N. C. (2000). Solid-State 13C and 31P NMR Analysis of Urinary Stones. *J. Urol.*, *164*(September), 856–863. https://doi.org/10.1016/S0022-5347(05)67327-2

Baran, E. J. (2015). Plant Physiology, *128*(2), 707–713. https://doi.org/10.1104/pp.010630.Some

Barber, V. C.; Dilly, P. N. (1969). Some aspects of the fine structure of the statocysts of the molluscs Pecten and Pterotrachea. *Zeitschrift Für Zellforschung Und Mikroskopische Anatomie*, *94*(4), 462–478. https://doi.org/10.1007/BF00936053

Barroso, C. M., Nunes, M., Richardson, C. A., & Moreira, M. H. (2005). The gastropod statolith: a tool for determining the age of Nassarius reticulatus. *Marine Biology*, *146*(6), 1139–1144. https://doi.org/10.1007/s00227-004-1516-2

Bayne, B. L. (1976). *Marine Mussels: Their Ecology and Physiology*. (B. L. Bayne, Ed.) (1st ed.). Cambridge University Press.

Campana, S. E. (1999). Chemistry and composition of fish otoliths:pathways, mechanisms and applications. *Marine Ecology Progress Series*, *188*(6), 263–297. https://doi.org/10.3354/meps188263

Campbell, A. K. (2017). *Fundamentals of Intracellular Calcium*.

Carregosa, V., Velez, C., Soares, A. M. V. M., Figueira, E., & Freitas, R. (2014). Physiological and

biochemical responses of three Veneridae clams exposed to salinity changes. *Comparative Biochemistry and Physiology Part - B: Biochemistry and Molecular Biology*, *177–178*, 1–9. https://doi.org/10.1016/j.cbpb.2014.08.001

Chatzinikolaou, E., & Richardson, C. (2007a). Evaluating growth and age of netted whelk Nassarius reticulatus (Gastropoda: Nassariidae) using statolith growth rings. *Marine Ecology Progress Series*, *342*, 163–176. https://doi.org/10.3354/meps342163

Chatzinikolaou, E., & Richardson, C. (2007b). Evaluating growth and age of netted whelk Nassarius reticulatus (Gastropoda: Nassariidae) using statolith growth rings. *Marine Ecology Progress Series*, *342*(August 2014), 163–176. https://doi.org/10.3354/meps342163

Chessa, G., Serra, S., Saba, S., Manca, S., Chessa, F., Trentadue, M., & Fois, N. (2013). The floating upwelling system (FLUPSY) for breeding of venerupis decussata (linnaeus, 1758) juveniles in a coastal lagoon in sardinia (Italy). *Transitional Waters Bulletin*, *7*(2), 53–61. https://doi.org/10.1285/i1825229Xv7n2p53

Chia, F. S., Koss, R., & Bickell, L. R. (1981). Fine structural study of the statocysts in the veliger larva of the nudibranch, Rostanga pulchra. *Cell and Tissue Research*, *214*(1), 67–80. https://doi.org/10.1007/BF00235145

Clarke, M. R. (1978). The cephalopod statolith - an introduction to its form. *Journal of the Marine Biological Association of the United Kingdom*, *58*(3), 701–712. https://doi.org/10.1017/S0025315400041345

Conti, C., Casati, M., Colombo, C., Possenti, E., Realini, M., Gatta, G. D., … Zerbi, G. (2015a). Synthesis of calcium oxalate trihydrate: New data by vibrational spectroscopy and synchrotron X-ray diffraction. *Spectrochimica Acta - Part A: Molecular and Biomolecular Spectroscopy*, *150*, 721–730. https://doi.org/10.1016/j.saa.2015.06.009

Conti, C., Casati, M., Colombo, C., Possenti, E., Realini, M., Gatta, G. D., … Zerbi, G. (2015b). Synthesis of calcium oxalate trihydrate: New data by vibrational spectroscopy and synchrotron X-ray diffraction. *Spectrochimica Acta - Part A: Molecular and Biomolecular Spectroscopy*, *150*, 721–730. https://doi.org/10.1016/j.saa.2015.06.009

Cragg, S. M., & Nott, J. A. (1977). The ultrastructure of the statocysts in the pediveliger larvae of Pecten maximus (L.) (Bivalvia). *Journal of Experimental Marine Biology and Ecology*, *27*(1), 23–36. https://doi.org/10.1016/0022-0981(77)90051-X

Edwards, H. G. M., Farwell, D. W., Jenkins, R., & Seaward, M. R. D. (1992). Vibrational Raman spectroscopic studies of calcium oxalate monohydrate and dihydrate in lichen encrustations on renaissance frescoes. *Journal of Raman Spectroscopy*, *23*(3), 185–189.

https://doi.org/10.1002/jrs.1250230310

Forsythe, J. W. (2004). Accounting for the effect of temperature on squid growth in nature: From hypothesis to practice. *Marine and Freshwater Research*, *55*(4), 331–339. https://doi.org/10.1071/MF03146

Forsythe, J. W., Derusha, R. H., & Hanlon, R. T. (1994). Growth, Reproduction and Life-Span of Sepia-Officinalis (Cephalopoda, Mollusca) Cultured Through 7 Consecutive Generations. *Journal of Zoology*, *233*, 175–192.

Forsythe, J. W., & Hanlon, R. T. (1988). and life span of Octopus bimaculoides. *Marine Biology*, *379*, 369–379. https://doi.org/10.1007/BF00391113

Frausto-Reyes, C., Loza-Cornejo, S., Terrazas, T., Miranda-Beltran, M. D., Aparicio-Fernandez, X., Lopez-Macias, B. M., … Ortiz-Morales, M. (2014). Raman Spectroscopy Study of Calcium Oxalate Extracted from Cacti Stems. *Applied Spectroscopy*, *68*(11), 1260–1265. https://doi.org/10.1366/14-07485

Fuchs, H. L., Christman, A. J., Gerbi, G. P., Hunter, E. J., & Diez, F. J. (2015). Directional flow sensing by passively stable larvae. *Journal of Experimental Biology*, *218*(17), 2782–2792. https://doi.org/10.1242/jeb.125096

Galante-Oliveira, S., Marçal, R., Espadilha, F., Sá, M., Abell, R., Machado, J., & Barroso, C. M. (2015). Detection of periodic Sr Ca−1 cycles along gastropod statoliths allows the accurate estimation of age. *Marine Biology*, *162*(7), 1473–1483. https://doi.org/10.1007/s00227-015-2684-y

Galante-Oliveira, S., Marçal, R., Guimarães, F., Soares, J., Lopes, J. C., Machado, J., & Barroso, C. (2014). Crystallinity and microchemistry of Nassarius reticulatus (Caenogastropoda) statoliths: Towards their structure stability and homogeneity. *Journal of Structural Biology*, *186*(2), 292–301. https://doi.org/10.1016/j.jsb.2014.03.023

Galante-Oliveira, S., Marcal, R., Ribas, F., Machado, J., & Barroso, C. (2013). Studies on the morphology and growth of statoliths in Caenogastropoda. *Journal of Molluscan Studies*, *79*(4), 340–345. https://doi.org/10.1093/mollus/eyt028

Galante-Oliveira, Marçal, R., Guimarães, F., Machado, J., & Barroso, C. M. (2013). The Gastropod Statolith Elemental Composition by EMPA. *Microscopy and Microanalysis*, *19*(S4), 87–88. https://doi.org/10.1017/S1431927613001050

Galtsoff, P. . (1964). The American oyster Crassostrea virginica Gmelin. *Fishery Bulletin*, *64*, 480. https://doi.org/10.1037/11766-016

Gao, W., & Wiederhold, M. L. (1997). The structure of the statocyst of the freshwater snail

Biomphalaria glabrata (Pulmonata, Basommatophora). *Hearing Research*, *109*(1–2), 109–124. https://doi.org/10.1016/S0378-5955(97)00058-0

Gaspar, M. B., Castro, M., & Monteiro, C. C. (1995). Age and growth rate of the clam, spisula solida L., from a site off Vilamoura, south Portugal, determined from acetate replicas of shell sections. *Scientia Marina*, *59*, 87–93.

Gosling, E. (Ed.). (2003). *Bivalve Molluscs*. Oxford, UK: Blackwell Publishing Ltd. https://doi.org/10.1002/9780470995532

Grana-Raffucci, F. A., & Appeldoorn, R. S. (1997). Age determination of larval strombid gastropods by means of growth increment counts in statoliths. *Fishery Bulletin*, *95*(4), 857–862.

Hajir, M., Graf, R., & Tremel, W. (2014). Stable amorphous calcium oxalate: synthesis and potential intermediate in biomineralization. *Chem. Commun.*, *50*(49), 6534–65366. https://doi.org/10.1039/c4cc02146k

Harris, J. (1932). Chapter XVI. In *Philosophical arrangements.* (Vol. 64, pp. 381–405). London: John Nourse. https://doi.org/10.1037/11766-016

Hollyman, P., Leng, M., Chenery, S., Laptikhovsky, V., & Richardson, C. (2017). Statoliths of the whelk Buccinum undatum: a novel age determination tool. *Marine Ecology Progress Series*, *AdvanceVie*(January), 1–12. https://doi.org/10.3354/meps12119

Hug, S., Grohe, B., Jalkanen, J., Chan, B., Galarreta, B., Vincent, K., … Hunter, G. K. (2012). Mechanism of inhibition of calcium oxalate crystal growth by an osteopontin phosphopeptide. *Soft Matter*, *8*(4), 1226–1233. https://doi.org/10.1039/C1SM06232H

Jakubik, B. (2012). Life strategies of Viviparidae (Gastropoda: Caenogastropoda: Architaenioglossa) in various aquatic habitats: <i>Viviparus viviparus</i> (Linnaeus, 1758) and <i>V. contectus</i> (Millet, 1813). *Folia Malacologica*, *20*(3), 145–179. https://doi.org/10.2478/v10125-012-0013-3

Jara-Jara, R., Pazos, A. J., Abad, M., García-Marťin, L. O., & Sánchez, J. L. (1997). Growth of clam seed (Ruditapes decussatus) reared in the wastewater effluent from a fish farm in Galicia (N.W. Spain). *Aquaculture*, *158*(3–4), 247–262. https://doi.org/10.1016/S0044-8486(97)00196-8

Jordan, E. L., & Verma, P. S. (1963). Invertibrate Zoology.

Kondrachuk, A. V., & Wiederhold, M. L. (2004). On generation of statoconia in gravireceptors of mollusks. *Hearing Research*, *197*(1–2), 24–34. https://doi.org/10.1016/j.heares.2004.06.001

Lacoue-Labarthe, T., Réveillac, E., Oberhänsli, F., Teyssié, J. L., Jeffree, R., & Gattuso, J. P. (2011). Effects of ocean acidification on trace element accumulation in the early-life stages of squid

Loligo vulgaris. *Aquatic Toxicology*, *105*(1–2), 166–176. https://doi.org/10.1016/j.aquatox.2011.05.021

Liu, B. L., Cao, J., Truesdell, S. B., Chen, Y., Chen, X. J., & Tian, S. Q. (2016). Reconstructing cephalopod migration with statolith elemental signatures: a case study using Dosidicus gigas. *Fisheries Science*, *82*(3), 425–433. https://doi.org/10.1007/s12562-016-0978-8

Maneja, R. H., Piatkowski, U., & Melzner, F. (2011). EFFECTS OF OCEAN ACIDIFICATION ON STATOLITH CALCIFICATION AND PREY CAPTURE IN EARLY LIFE CUTTLEFISH,Sepia officinalis. *Journal of Shellfish Research*, *15*(4), 7–10. Retrieved from %3CGo

Manríquez, P. H., Galaz, S. P., Opitz, T., Hamilton, S., Paradis, G., Warner, R. R., … Lagos, N. A. (2012). Geographic variation in trace-element signatures in the statoliths of near-hatch larvae and recruits of Concholepas concholepas (loco). *Marine Ecology Progress Series*, *448*, 105–118. https://doi.org/10.3354/meps09514

Morton, B. (1985). Statocyst structure in the Anomalodesmata (Bivalvia). *Journal of Zoology*, *206*(1), 23–34. https://doi.org/10.1111/j.1469-7998.1985.tb05633.x

Morton, B. (1996). The biology and functional morphology of Minnivola pyxidatus (Bivalvia: Pectinoidea). *Journal of Zoology*, *240*(4), 735–760. https://doi.org/10.1111/j.1469-7998.1996.tb05318.x

Moss, D. K., Ivany, L. C., Judd, E. J., Cummings, P. W., Bearden, C. E., Kim, W.-J., … Alroy, J. (2016). Lifespan, growth rate, and body size across latitude in marine Bivalvia, with implications for Phanerozoic evolution. *Proceedings. Biological Sciences / The Royal Society*, *283*(1836), 867–870. https://doi.org/10.1098/rspb.2016.1364

Nehrke, G., & Nouet, J. (2011). Confocal Raman microscope mapping as a tool to describe different mineral and organic phases at high spatial resolution within marine biogenic carbonates: Case study on Nerita undata (Gastropoda, Neritopsina). *Biogeosciences*, *8*(12), 3761–3769. https://doi.org/10.5194/bg-8-3761-2011

Neumeister, H., & Budelmann, B. U. (1997). Structure and function of the Nautilus statocyst. *Philosophical Transactions of the Royal Society B: Biological Sciences*, *352*(1361), 1565–1588. https://doi.org/10.1098/rstb.1997.0142

Overnell, J. (1981). Protein and oxalate in mineral granules from the kidney of Pecten maximus (L.). *Journal of Experimental Marine Biology and Ecology*, *52*(2–3), 173–183. https://doi.org/10.1016/0022-0981(81)90035-6

Passos, F. D., & Machado, F. M. (2014). A New Species of Cyamiocardium Soot-Ryen, 1951 from Shallow Waters off Brazil, with a Discussion on the Anatomical Characters of the Cyamiidae

(Bivalvia: Cyamioidea). *American Malacological Bulletin*, *32*(1), 122–131. https://doi.org/10.4003/006.032.0110

Pecl, G. T., Doubleday, Z. A., Danyushevsky, L., Gilbert, S., & Moltschaniwskyj, N. A. (2010). Transgenerational marking of cephalopods with an enriched barium isotope: A promising tool for empirically estimating post-hatching movement and population connectivity. *ICES Journal of Marine Science*, *67*(7), 1372–1380. https://doi.org/10.1093/icesjms/fsq025

Pedrozo, H. A., Schwartz, Z., Dean, D. D., Wiederhold, M. L., & Boyan, B. D. (1996). Regulation of statoconia mineralization in Aplysia californica in vitro. *Connect Tissue Res*, *35*(1–4), 317–323. https://doi.org/10.3109/03008209609029206

Radtke, R. L. (1983). Chemical and structural characteristics of statoliths from the short-finned squid Illex illecebrosus. *Marine Biology*, *76*(1), 47–54. https://doi.org/10.1007/BF00393054

Richardson, C. A. (2001). Molluscs as archives of environmental change. In *Oceanography and Marine Biology, An annual review* (Vol. 39, pp. 103–164).

Richardson, C. A., Kingsley-Smith, P. R., Seed, R., & Chatzinikolaou, E. (2005). Age and growth of the naticid gastropod Polinices pulchellus (Gastropoda: Naticidae) based on length frequency analysis and statolith growth rings. *Marine Biology*, *148*(2), 319–326. https://doi.org/10.1007/s00227-005-0072-8

Rodhouse, P. G., & Hatfield, E. M. C. (1990). Age determination in squid using statolith growth increments. *Fisheries Research*, *8*(4), 323–334. https://doi.org/10.1016/0165-7836(90)90002-D

Sartori, A. F.; Domaneschi, O. (2005). The functional morphology of the antarctic bivalve Thracia meridionalis Smith, 1885 (Anomalodesmata: Thraciidae). *Journal of Molluscan Studies*, *71*(3), 199–210. https://doi.org/10.1093/mollus/eyi028

Semmens, J. M., Pecl, G. T., Gillanders, B. M., Waluda, C. M., Shea, E. K., Jouffre, D., … Shaw, P. W. (2007). Approaches to resolving cephalopod movement and migration patterns. *Reviews in Fish Biology and Fisheries*, *17*(2–3), 401–423. https://doi.org/10.1007/s11160-007-9048-8

Simone, L. R. L. (2009). Anatomical description of Solen cf. exiguus Dunker from Thailand (Bivalvia: Solenidae). *Archiv Für Molluskenkunde: International Journal of Malacology*, *138*(2), 113–122. https://doi.org/10.1127/arch.moll/1869-0963/138/113-122

Sobral, P., & Widdows, J. (1997). Influence of hypoxia and anoxia on the physiological responses of the clam Ruditapes decussatus from southern Portugal. *Marine Biology*, *127*(3), 455–461. https://doi.org/10.1007/s002270050033

Villanueva, R. (2000). Effect of temperature on statolith growth of the European squid Loligo

vulgaris during early life. *Marine Biology*, *136*(3), 449–460. https://doi.org/10.1007/s002270050704

Wehrmeister, U., Jacob, D. E., Soldati, A. L., Loges, N., Häger, T., & Hofmeister, W. (2011). Amorphous, nanocrystalline and crystalline calcium carbonates in biological materials. *Journal of Raman Spectroscopy*, *42*(5), 926–935. https://doi.org/10.1002/jrs.2835

Wheeler, J. D., Helfrich, K. R., Anderson, E. J., & Mullineaux, L. S. (2015). Isolating the hydrodynamic triggers of the dive response in eastern oyster larvae. *Limnology and Oceanography*, *60*(4), 1332–1343. https://doi.org/10.1002/lno.10098

Wiederhold, M. L., Sharma, J. S., Driscoll, B. P., & Harrison, J. L. (1990). Development of the statocyst in Aplysia californica I. Observations on statoconial development. *Hearing Research*, *49*(1–3), 63–78. https://doi.org/10.1016/0378-5955(90)90095-7

Young, C. M., Sewell, M. A., & Rice (eds), Academic Press, M. E. (2003). Atlas of Marine Invertebrate Larvae. *Aquaculture Research*, *34*(5), 437–437. https://doi.org/10.1046/j.1365-2109.2003.00819.x

Zacherl, D. (2005). Spatial and temporal variation in statolith and protoconch trace elements as natural tags to track larval dispersal. *Marine Ecology Progress Series*, *290*, 145–163. https://doi.org/10.3354/meps290145

Zhang, Y., Shi, F., Song, J., Zhang, X., & Yu, S. (2015). Hearing characteristics of cephalopods: Modeling and environmental impact study. *Integrative Zoology*, *10*(1), 141–151. https://doi.org/10.1111/1749-4877.12104

Zumholz, K., Hansteen, T. H., Klügel, A., & Piatkowski, U. (2006). Food effects on statolith composition of the common cuttlefish (Sepia officinalis). *Marine Biology*, *150*(2), 237–244. https://doi.org/10.1007/s00227-006-0342-0